ACS OMEGA

http://pubs.acs.org/journal/acsodf

Article

Multifactor Prediction of the Water Richness of Coal Roof Aquifers Based on the Combination Weighting Method and TOPSIS Model: A Case Study in the Changcheng No. 1 Coal Mine

Mei Qiu, Xinyu Yin, Longqing Shi,* Peihe Zhai, Guichao Gai, and Zhendong Shao

Cite This: *ACS Omega* 2022, 7, 44984−45003

Read Online

ACCESS | Metrics & More | Article Recommendations | Supporting Information

ABSTRACT: Identifying the water richness of coal roof aquifers is an important and difficult goal of hydrogeological research to prevent and control roof water disasters. To evaluate the water richness of roof sandstone aquifers of the No. 1 coal seam in the Changcheng No. 1 coal mine, a multifactor prediction method based on the fuzzy Delphi analytic hierarchy process (FDAHP), entropy weight method (EWM), sum of squared deviations (SSD), and Technique for Order Preference by Similarity to an Ideal Solution (TOPSIS) was proposed. Multisource geological data, including sandstone thickness, burial depth, lithological composition index, core recovery, fault scale index, fault intersections and endpoint density, and fold fractal dimension, were chosen as the primary indicators for evaluating the water richness of roof sandstone aquifers. The FDAHP and EWM were used to scientifically determine the subjective and objective weight vectors of these seven main factors, and the SSD was used to determine the optimal combination weights based on the objective and subjective weight vectors. On this basis, the water richness index (WRI) model was developed using the TOPSIS method to rank the water richness of samples in the study area. A water richness zoning map was created using the WRI values, revealing three zones: the weak water richness zone, moderate water richness zone, and strong water richness zone. Additionally, the map was refined by incorporating hydrogeologic data collected during mining operations, including pumping tests and actual water inrushes from roadways and working faces. It is believed that the proposed WRI model is effective for predicting the water richness of the roof sandstone aquifers of the No. 1 coal seam in the Changcheng No. 1 coal mine based on the engineering practice data used to validate the WRI model.

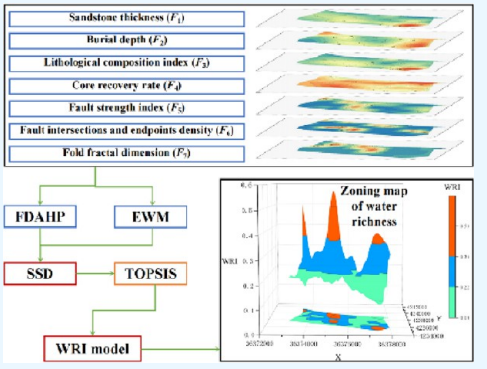

1. INTRODUCTION

During coal mining and tunnel excavation, a large amount of water inrush may occur, posing risks to the project. According to incomplete statistics, between 2011 and 2020, there were 95 coal mine flood accidents in China, which caused 536 deaths, including 50 relatively serious flood accidents and 18 serious flood accidents.[1] Accordingly, mine water hazards have been a major challenge for coal mine safety production in the coal industry. Further, roof water inrush is one of the most prevalent and direct major threats to safe mining in China. The water richness of the roof aquifer directly determines the occurrence and quantity of roof water inrush. To guide the prevention and control of coal floor water damage, it is necessary to evaluate the water richness of the aquifer on a real-world basis and to demarcate the rich water partition.

Traditional approaches to determine the water richness of an aquifer include pumping tests and geophysical prospecting. Although these approaches are widely used to evaluate the water richness of aquifers, they are typically expensive and time consuming and have a restricted control range. The water richness of the roof aquifer is usually influenced by multiple geoscience factors, including geology, hydrogeology, and tectonic geology. Many scholars have conducted studies that consider multiple factors to assess the water richness of the roof aquifer. Common methods include the entropy weight method (EWM), water-rich index model based on the GIS information fusion principle, backpropagation (BP) neural network method, fuzzy clustering comprehensive evaluation method, analytic hierarchy process (AHP), variation coefficient method, triangular fuzzy number (TFN), and fuzzy Delphi analytic hierarchy process (FDAHP).[2−10] The main idea of establishing the multifactor evaluation model of roof aquifer water richness is to establish the index system of aquifer water richness influencing factors and then employ one or more methods to determine the relative weight of various factors. However, the existing comprehensive evaluation methods have limitations in the evaluation process. For example, the AHP

Received: August 18, 2022
Accepted: November 18, 2022
Published: November 29, 2022

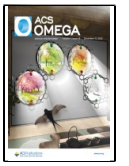

https://doi.org/10.1021/acsomega.2c05297
ACS Omega 2022, 7, 44984−45003

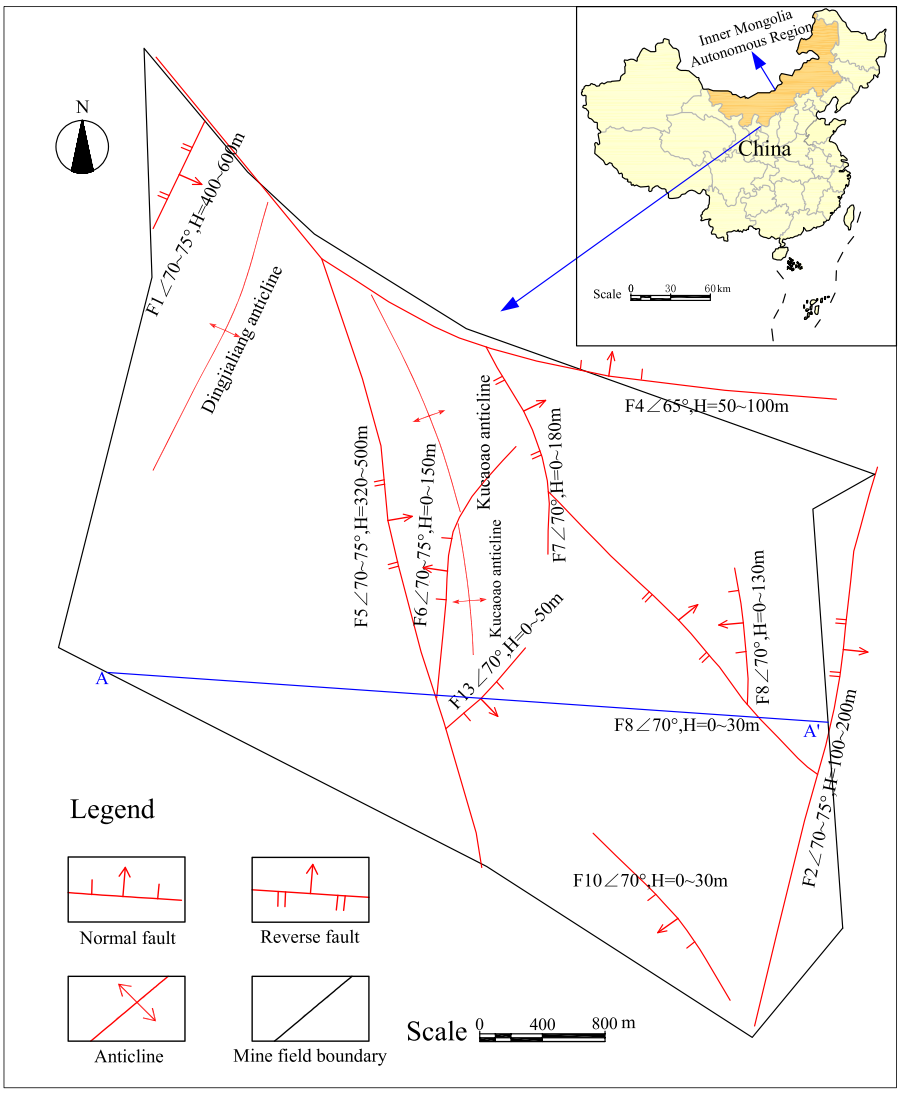

Figure 1. Location and geologic structures of the study area in Inner Mongolia Autonomous Region, China.

method is primarily used to assign subjective weights to each factor during the evaluation process. The EWM and variation coefficient method weighted the factors based on the characteristics of the original data of the factors; despite being relatively objective methods, the results do not accurately reflect the relationship between the factors and water richness of an aquifer. The majority of the prediction methods are based on linear weighting; however, the prediction of water richness is a system problem with intricate internal mechanisms. The BP neural network method provides nonlinear modeling for water richness prediction; however, this method is limited by the number of predicted samples, and the prediction error is large when data is insufficient.

Herein, based on a comprehensive analysis of existing multisource geological information, a multifactor prediction method was proposed using the FDAHP, EWM, sum of squared deviations (SSD), and Technique for Order Preference by Similarity to an Ideal Solution (TOPSIS). The multisource factor weights were determined using FDAHP, EWM, and SSD. FDAHP is a fuzzy group decision-making method that combines the fuzzy evaluation principle, AHP, and Delphi group decision-making method to eliminate the ambiguity and subjectivity of expert opinions regarding the relative importance of the factors. EWM assigns weight by calculating the amount of information on indicators, a technique that is commonly used in multi-index evaluation; the greater the information, the greater the weight, and vice versa.[11,12] The primary advantage of the EWM over the AHP is that it eliminates the interference of subjective factors and ensures the objectivity of the weight.[13,14] Using the SSD, subjective and objective weights were combined. Based on this, the TOPSIS method was used to establish the water richness index (WRI), which can be used to rank the water richness of the samples in the study area. The TOPSIS method is a nonlinear method widely used in multi-attribute decision-making analysis and ranks the degree of water richness in the study area. This study is unique in its use of the combination weighting method and the TOPSIS model to predict the roof aquifer water richness.

2. STUDY AREA AND GEOLOGIC AND HYDROGEOLOGICAL SETTINGS

2.1. Study Area. The Changcheng No. 1 coal mine is located in Shanghai Miao Town, Ertok Qianqi, Ordos City, Inner Mongolia Autonomous Region at 106°32′40″−

https://doi.org/10.1021/acsomega.2c05297
ACS Omega 2022, 7, 44984−45003

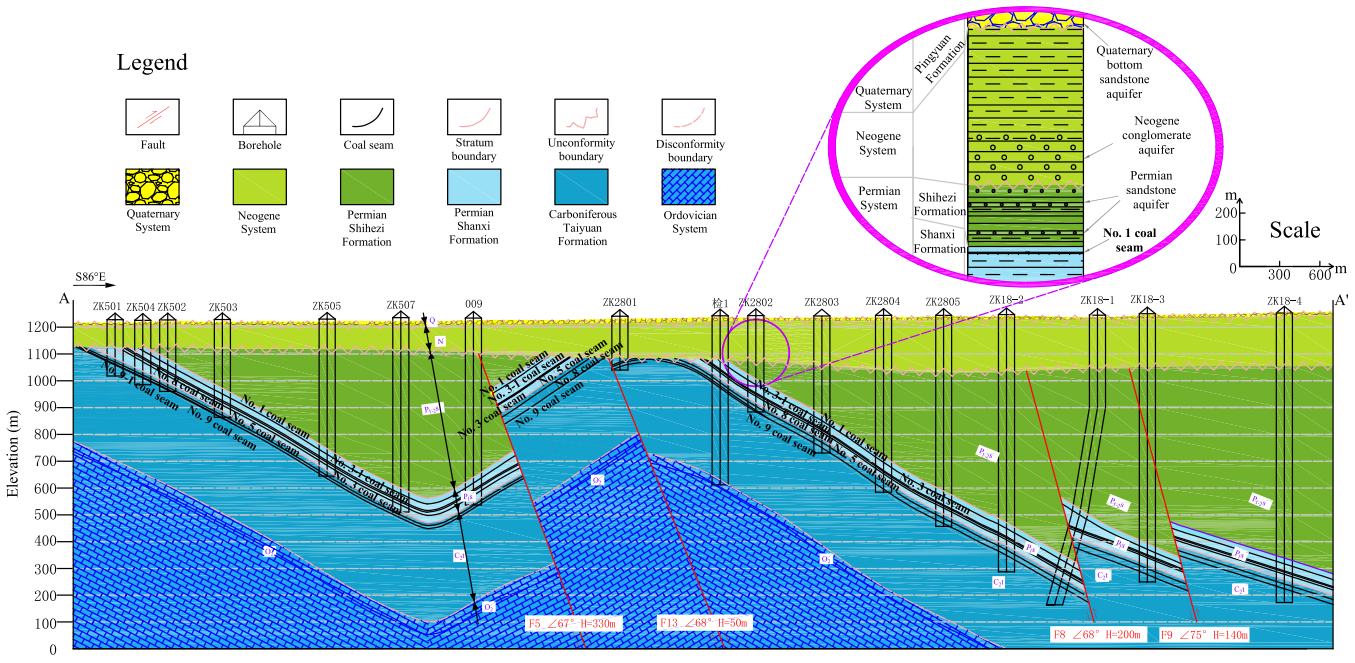

Figure 2. Geological profile of A-A′.

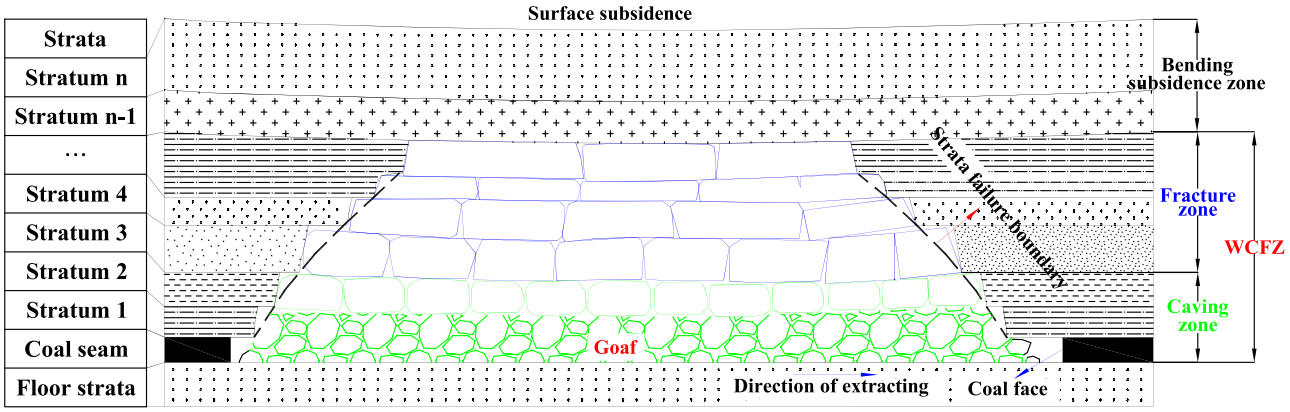

Figure 3. Division diagram of the "upper three zones" of the roof of the mining coal seam.

106°37′04″ East and 38°14′26″−38°17′16″ North, as shown in Figure 1.

The study area belongs to the Ordos Plateau and has a gentle topography, ground elevation +1090 to +1247 m that is high in the east and low in the west, and sparse vegetation. The climate is a northern temperate continental climate, a semi-arid desert climate zone, with perennial drought and water shortage. The average annual precipitation is 270.40 mm, with the rainy season occurring between July and September with heavy rainfall; the annual evaporation exceeds 2465 mm. Typically, it freezes in late October and thaws in March of the following year. Approximately 1000 m south of the coal mine in Ningxia is the Biangou River that flows northwest into the Yellow River. The Yellow River is about 14 km away from the area in a straight line, with a water level of about 1100 m.

2.2. Geological Conditions. The stratigraphy of the Changcheng No. 1 coal mine is roughly north−south-oriented and dips eastward by 5°−35°. Folding and fracture structures are well-developed in the field. There are two folds in the field, namely, the Dingjialiang and Kucaoao anticlines. There are 10 large and moderate-sized faults in the field. The majority of the faults have a large dip angle, including the F5 fault, which has a large drop and a long extension, as shown in Figure 1.

The Changcheng No.1 coal mine has developed Ordovician, Carboniferous, Permian, Neogene, and Quaternary formations, as shown in Figure 2. The coal-bearing strata in the field are the Shanxi Formation and the Taiyuan Formation, containing a total of 12 coal seams, with the Shanxi Formation containing six coal seams (No. 1−6 coal seams) and the Taiyuan Formation containing six coal seams (No. 7−12 coal seams), with a total thickness of 6.96−20.94 m, averaging 14.88 m. There are seven recoverable or partially recoverable coal seams (No. 1, 3−1, 3, 5, 8, 9−1, and 9 coal seams), with a total thickness of 13.29 m on average.

2.3. Hydrogeological Conditions. The Changcheng No. 1 coal mine developed four major aquifers, namely, the pore aquifer of the Quaternary unconsolidated rock, the sandstone and conglomerate aquifers of the lower Neogene, the sandstone and thin limestone aquifers of the Carboniferous−Permian, and the Ordovician limestone aquifer. This study focuses on the No. 1 coal seam, which is currently one of the most heavily mined coal seams. The main aquifers above the

https://doi.org/10.1021/acsomega.2c05297
ACS Omega 2022, 7, 44984−45003

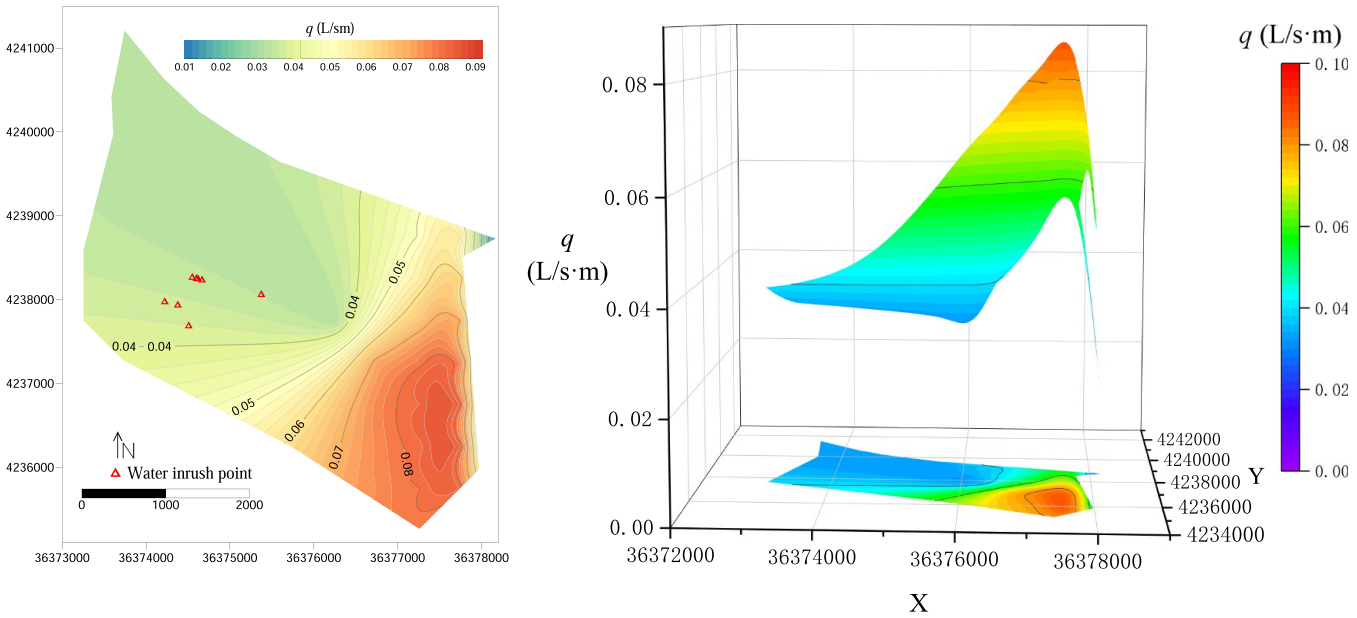

(a) Contour map (b) 3D surface map

Figure 4. Thematic map of the specific field *q*.

No. 1 coal seam include sand and gravel aquifers at the Quaternary strata, sandstone and conglomerate aquifers of the lower Neogene, and sandstone aquifers in the Shiqianfeng, Shihezi, and Shanxi groups of the Permian System. The primary aquitards are clay beds in the Neogene and mudstone, siltstone, and bauxite in the Permian System. Owing to the barrier of the aquitards, surface water, precipitation, and Quaternary water have no relationship with groundwater in the sandstone aquifers of the Permian System.

During the mining process of the No. 1 coal seam, the overburden strata of the No. 1 coal seam are deformed and destroyed, which can be divided into three zones (i.e., the upper three zones) based on the failure mode and degree of the overburden strata: the caving zone, fracture zone, and bending subsidence zone (Figure 3). The caving zone and fracture zone are collectively called the water-conducting fracture zone, where a large number of fractures are produced. The water-conducting fracture zone connects the coal roof sandstone aquifers to the working face and is the primary channel for aquifer water to enter the working area, as calculated using eqs 1 and 2 based on the *Regulations for Coal Pillar Retention and Pressed Coal Mining in Buildings, Water Bodies, Railways, and Main Roadways*.[15]

$$H = \frac{100M}{1.6\sum M + 3.6} \pm 5.6 \quad (1)$$

$$H = 20\sqrt{\sum M} + 10 \quad (2)$$

where H is the height of the water-conducting fracture zone, in meters, and M is the cumulative mining thickness of the No. 1 coal seam, in meters.

Therefore, the direct water-inrush aquifers for the No. 1 coal seam are the roof sandstone aquifers within the water-conducting fracture zone, which are the target aquifers for water richness evaluation. Hydraulic conductivities ranging from 0.0363 to 0.2979 m/day and specific fields (represented by q) ranging from 0.0320 to 0.0815 L/s·m were obtained via pumping tests on the sandstone aquifers in the No. S01, 2803, 2805, and X3 wells. According to the *Coal Mine Water Control Rules*,[16] the water richness of the roof sandstone aquifers of the No. 1 coal seam in the study area can be classified as a poor water richness zone based on the data q, the contour map, and the 3D surface map generated by Golden Software Surfer 13.0 and Origin software, as shown in Figure 4. However, during the extraction of the No. 1 coal seam, six medium-sized inrushes and one small-sized water inrush occurred. The occurrence of water inrushes is contradictory to the zones of water richness based on q as water inrushes are impossible in zones of low water richness during mining. Therefore, a comprehensive evaluation of the water richness of the roof aquifers is necessary for the safe mining of the No. 1 coal seam using available multisource geological, tectonic, and lithological data.

3. DATA USED

3.1. Selected Factors Affecting Water Richness of the Roof Aquifers. The existence and richness of groundwater in sandstone aquifers are controlled by many geo-environmental conditioning factors, including geological, tectonic, and lithological factors. To establish a water richness zoning map, a spatial database was considered as a set of conditioning factors that affect water richness. Seven conditioning factors were considered herein to develop a water richness prediction model and a water richness zoning map, including sandstone thickness (ST), burial depth (BD), lithological composition index (LCI), core recovery (CR), fault scale index (FSI), fault intersection and endpoint density (FIED), and fold fractal dimension (FFD). The data of the seven factors were collected and subsequently interpolated with the Kriging interpolation technique to create the contour map and 3D surface map by Golden Software Surfer 13.0 and Origin software.

3.2. Factors. *3.2.1. ST.* Usually, ST is one of the most important hydrogeological parameters. ST is the basis for the absolute water yield in the aquifer and can be used to evaluate

https://doi.org/10.1021/acsomega.2c05297
ACS Omega 2022, 7, 44984−45003

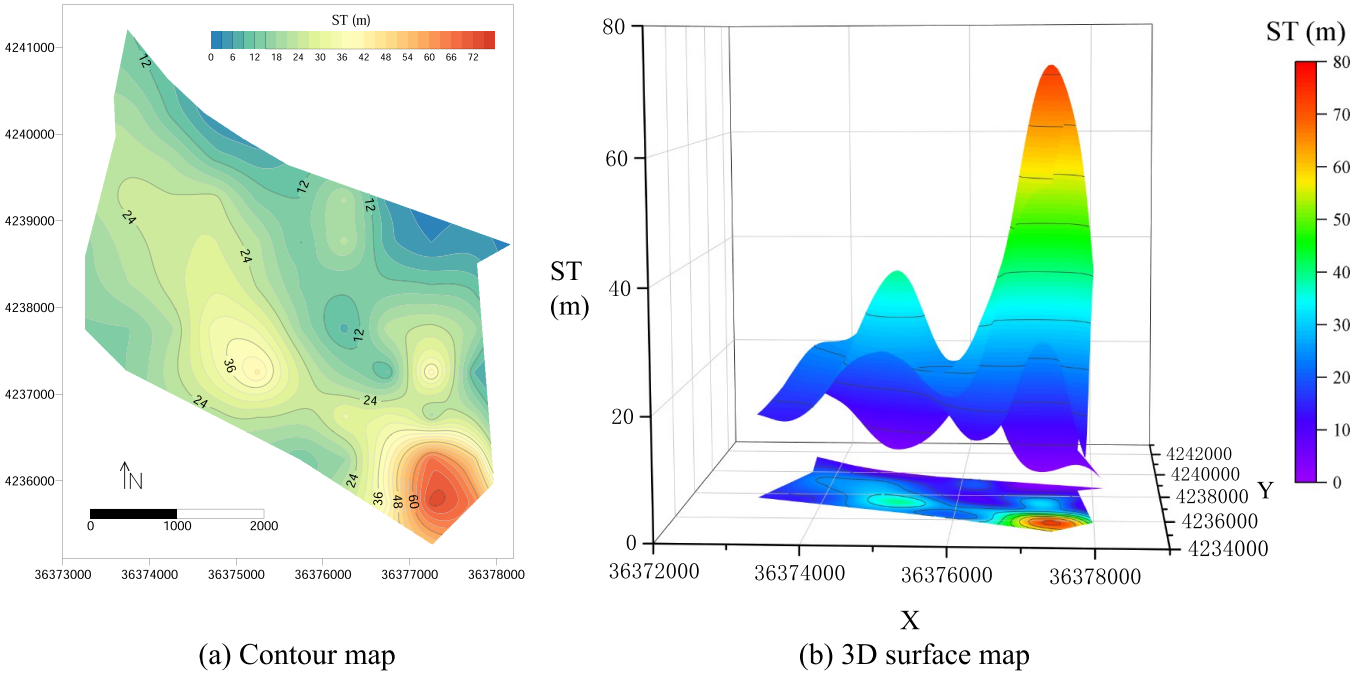

(a) Contour map (b) 3D surface map

Figure 5. Thematic map of sandstone thickness.

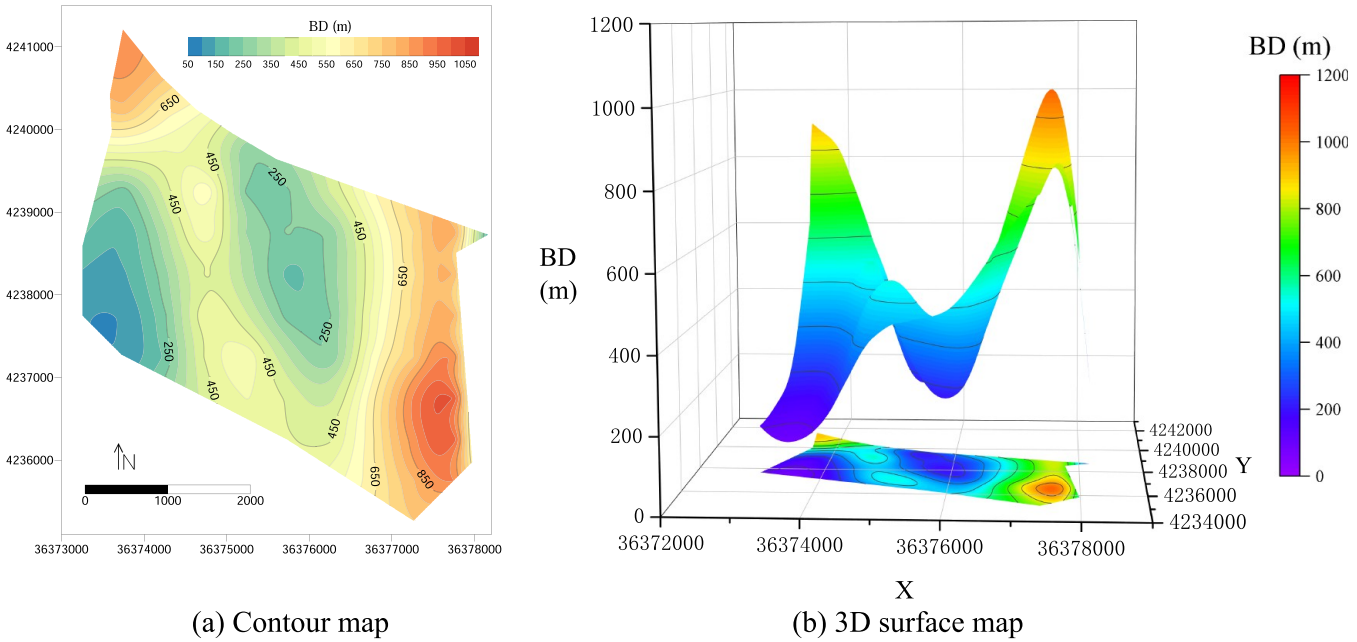

(a) Contour map (b) 3D surface map

Figure 6. Thematic map of burial depth.

the water richness of the aquifer. When all the other factors remain constant, the water yield increases with increasing aquifer thickness. ST was obtained from geo-exploration data, and the contour map and 3D surface map were generated displaying the distribution characteristics of the ST (Figure 5). The distribution of ST is highly variable, ranging from 0 to 58.2 m. The ST is greater in the west-central and southeastern regions of the study area, whereas it is less in the northern, central, and southwestern regions.

3.2.2. BD. The BD of the sandstone aquifers overlying the No. 1 coal seam affects the recharge condition of the groundwater. Groundwater in sandstone aquifers overlying the No. 1 coal seam is recharged at the outcrop surface, and as BD increases, the recharge conditions become progressively constrained. Additionally, increasing lithostatic pressure with increasing BD reduces connectivity by possibly closing the fractures. The BD of the sandstone aquifers was obtained through 3D-seismic exploration, geo-exploration, and workface and roadway construction, and the contour map and 3D surface map were generated, as shown in Figure 6.

3.2.3. LCI. The overlying strata of the No. 1 coal seam comprise clastic rocks, including conglomerate, sandstone of all grain sizes, and mudstone. Mudstone limits the development of fractures and hydraulic connections between sandstone aquifers, thereby decreasing the water storage capacity.[17,18] Previous studies indicate that the grain size of clastic rocks has

https://doi.org/10.1021/acsomega.2c05297
ACS Omega 2022, 7, 44984−45003

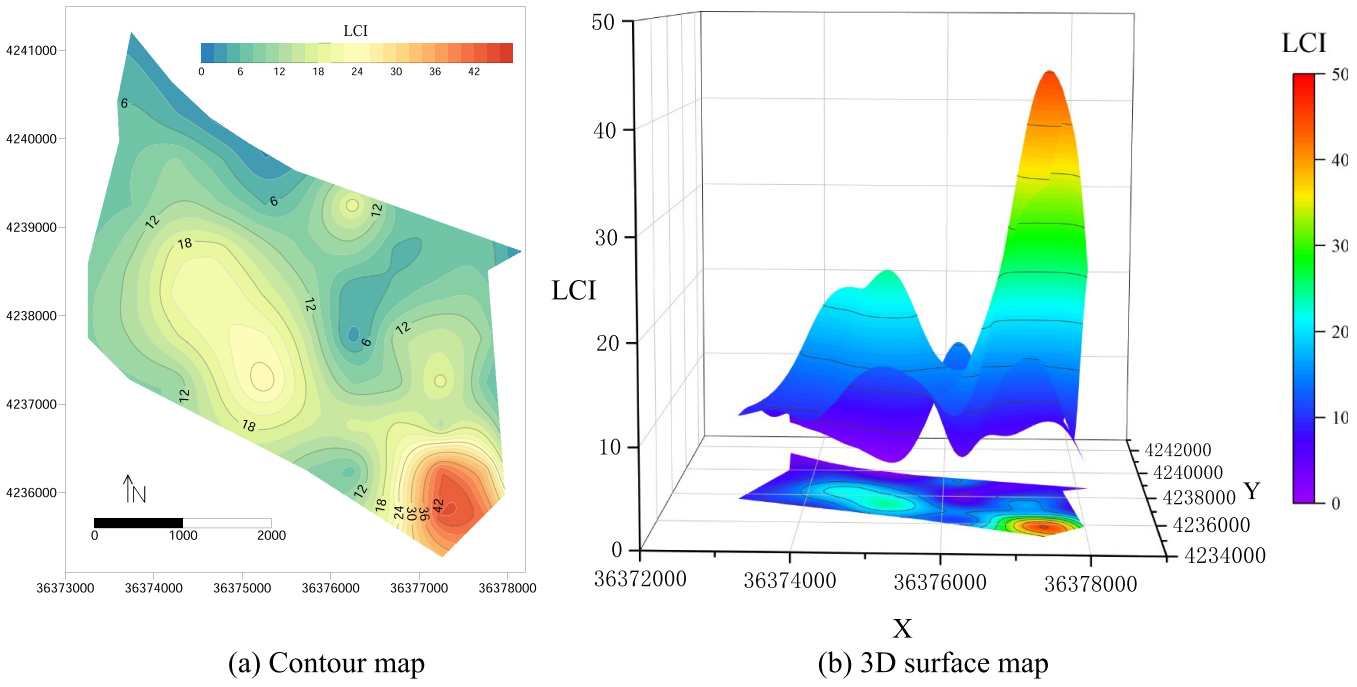

(a) Contour map (b) 3D surface map

Figure 7. Thematic map of the lithological composition index.

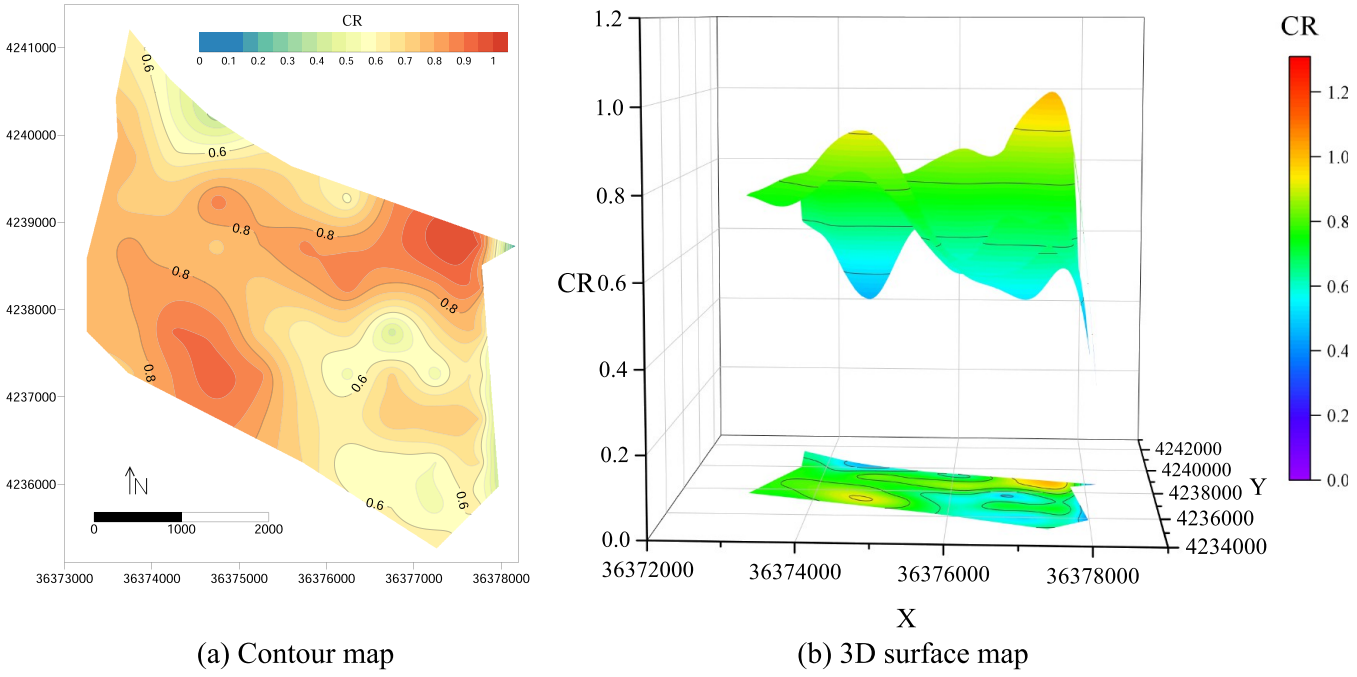

(a) Contour map (b) 3D surface map

Figure 8. Thematic map of core recovery.

a significant impact on the water richness of the aquifer; the coarser the clastic rocks, the greater their water storage capacity.[8] Conglomerate and sandstone are brittle and broken, yielding cracks that increase the permeability of the aquifer.[19] Therefore, LCI was proposed to incorporate the influence of various types of rocks overlying the No. 1 coal seam on the water richness of the roof aquifers.[8]

$$\mathrm{LCI} = (a \times 1 + b \times 0.8 + c \times 0.6 + d \times 0.4 + e \times 0.2 + f \times 1) \times g \quad (3)$$

where LCI is the lithological composition index; a, b, c, d, e, and f are the thicknesses of conglomerate, coarse sandstone, moderate sandstone, fine sandstone, siltstone, and fracture zones, respectively, in meters; 0.2, 0.4, 0.6, 0.8, and 1 are the equivalence coefficients for different rock types; and g is the structure coefficient. When the sandstone and conglomerate thickness exceed 80% of the total thickness, g = 1; when the proportion is between 55 and 80%, g = 0.8; when the proportion is between 45 and 55%, g = 0.6; when the proportion is between 20 and 45%, g = 0.4; and when the proportion is 20% or less, g = 0.2.[8] Based on the value

https://doi.org/10.1021/acsomega.2c05297
ACS Omega 2022, 7, 44984−45003

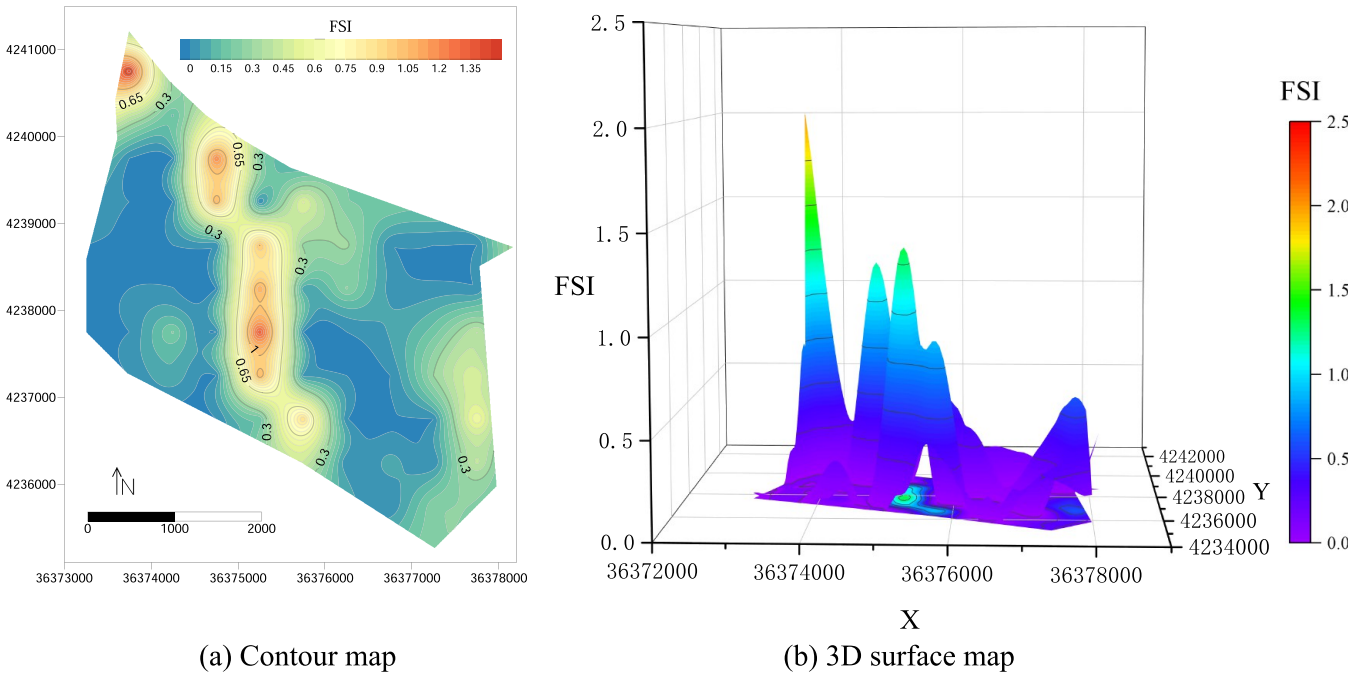

(a) Contour map (b) 3D surface map

Figure 9. Thematic map of the fault scale index.

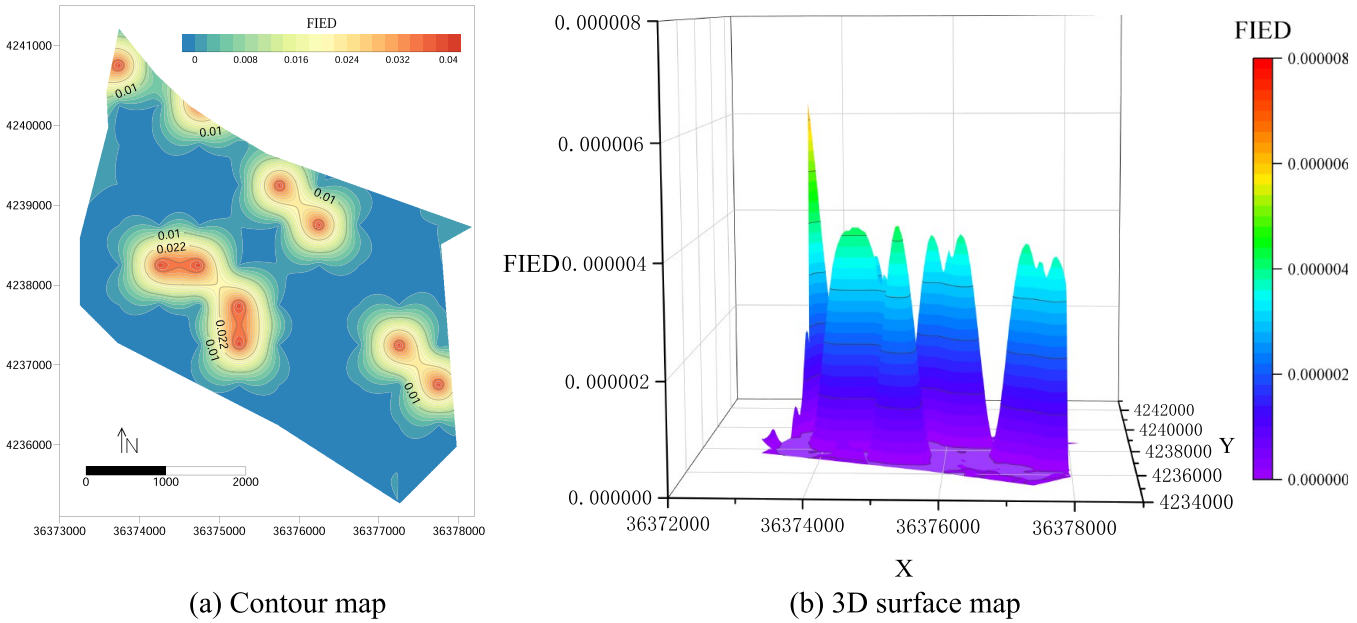

(a) Contour map (b) 3D surface map

Figure 10. Thematic map of the fault intersection and endpoint density.

calculation data of each exploration borehole, the contour map and 3D surface map were generated, as shown in Figure 7.

3.2.4. CR. The CR is the percentage of the core length to the drilling footage and is expressed by eq 4:

$$\mathrm{CR} = \frac{\sum a}{\sum A} \times 100\% \tag{4}$$

where CR is the core recovery; a is the core length, in meters; and A is the drilling footage, in meters.

CR, a rock quality index, reflects the integrity of a rock mass.[20] Under general conditions, the lower the CR of a sandstone formation, the more fragmented the rock is and the higher the groundwater connectivity. The CR was calculated based on the values in each exploratory borehole, and the contour map and 3D surface map were generated as shown in Figure 8.

3.2.5. FSI. Faults have a significant impact on groundwater potential as they provide storage space and migration channels for groundwater, which have traditionally been used as an indicator to evaluate the water richness of an aquifer. Faults are linear features of tectonic origin; they are long, narrow, and relatively straight, with parameters including fault dip angle, fault drop, and fault extension length. The greater the number and size of faults, the more storage space and the stronger the groundwater connection. The FSI was selected for the evaluation of aquifer water richness considering the extension

https://doi.org/10.1021/acsomega.2c05297
ACS Omega 2022, 7, 44984−45003

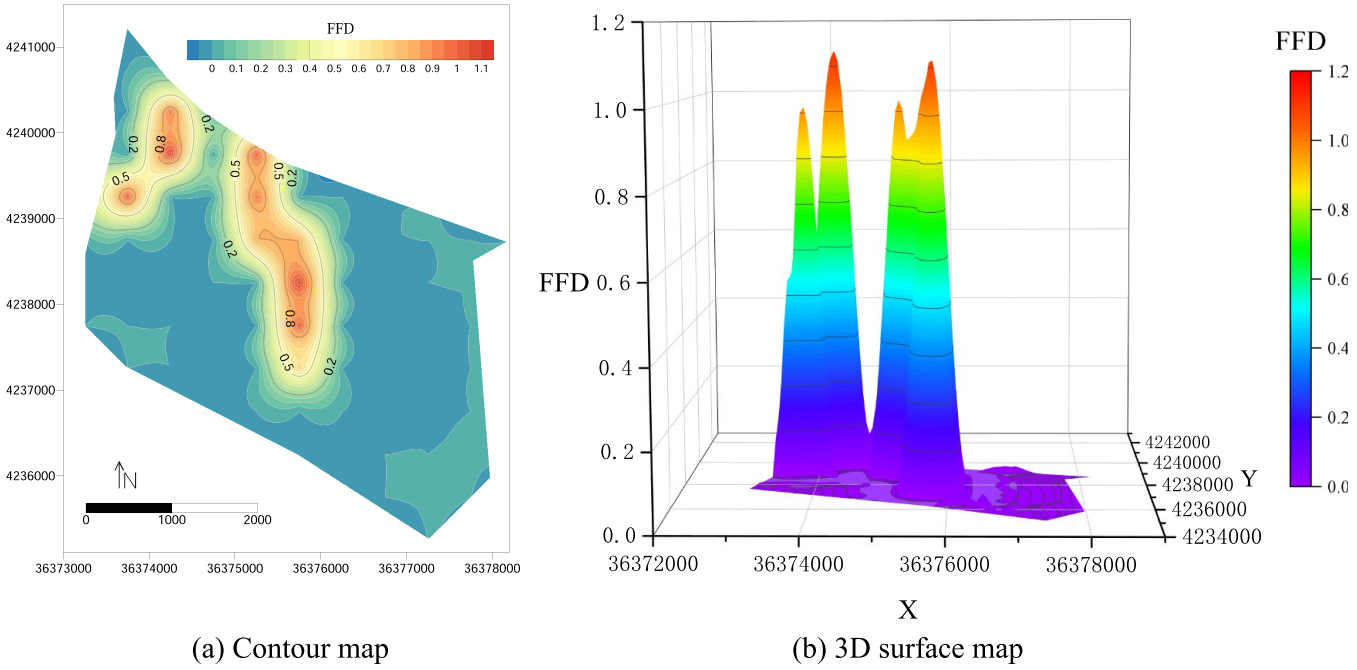

(a) Contour map (b) 3D surface map

Figure 11. Thematic map of the fold fractal dimension.

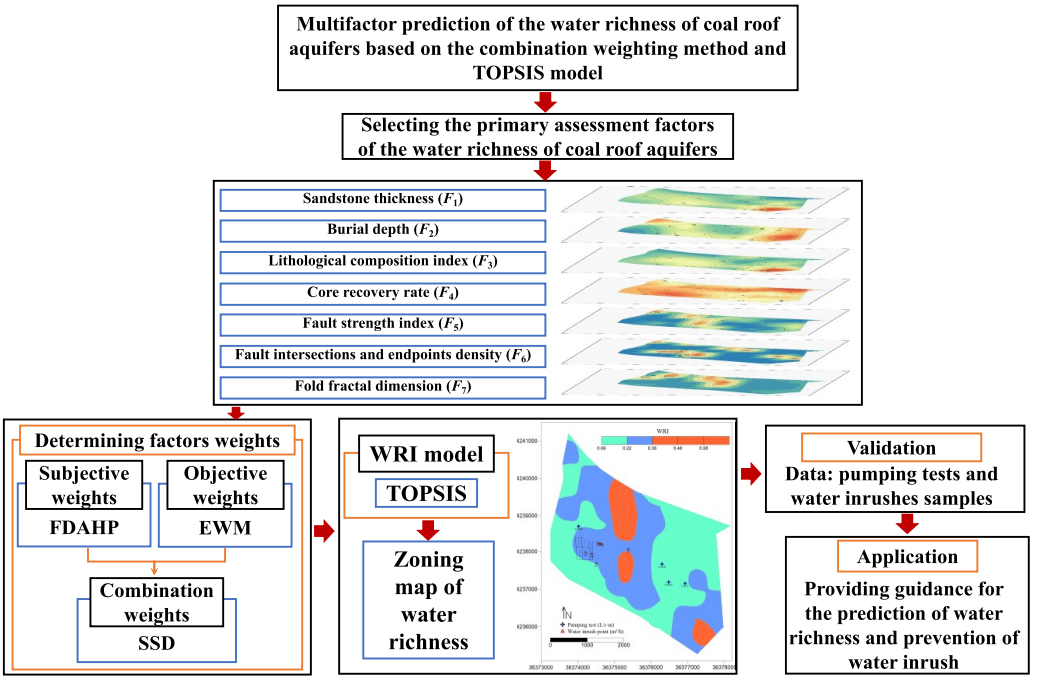

Figure 12. Study flow in this paper.

length and fault throw of all the faults in an evaluation unit. The FSI is expressed as follows:

$$\mathrm{FSI} = \frac{\sum_i^n l_i h_i}{S} \tag{5}$$

where FSI is the fault scale index, h is the fault throw, l is the corresponding strike length, S is the area of the grid cell, and n is the number of faults in the grid cell. The study area was first meshed into 500 m × 500 m grid cells, and subsequently the FSI was calculated in each grid cell based on the fault distribution characteristics using eq 5. The contour map and 3D surface map were generated, as shown in Figure 9.

3.2.6. FIED. Owing to the concentration of ground stress, the fault intersections and endpoints are more rock-broken. Therefore, the sandstone permeability and storage capacity increase with increasing intersections and endpoints. The fault intersection and endpoint density is indicated as follows:

$$\mathrm{FIED} = \frac{n}{S} \tag{6}$$

where FIED is the fault intersection and endpoint density, n is the total intersections and endpoints of all faults in the grid

https://doi.org/10.1021/acsomega.2c05297
ACS Omega 2022, 7, 44984−45003

cell, and S is the area of the grid cell. The value of FIED was calculated in each grid cell with a size of 500 m × 500 m, and the contour map and 3D surface map were generated, as shown in Figure 10.

3.2.7. FFD. Folds have a significant impact on groundwater potential primarily because a large number of tension fissures formed in the fold hinge zone provide groundwater with excellent storage space and migration channels. The degree of development of the fold structure can be quantified using the fractal dimension formula. The FFD was calculated as follows. The study area was first divided into 80 grid cells with a size of 500 m × 500 m, and every 500-m-long grid was subdivided into 250, 125, and 62.5 m subgrids; the number of grids with a fold axis passing through in each grid cell was counted to obtain the $N(r_i)$ values when r_1 = 500 m, r_2 = 250 m, r_3 = 125 m, and r_4 = 62.5 m; finally, the data of r_i and the corresponding $N(r_i)$ in each grid cell were put into the lg $N(r)$−lg R coordinate system to generate a fitting straight line, and the FFD in each grid cell, the absolute value of the slope of the line, was calculated using the least square method, as shown in eq 7.[21]

$$\mathrm{FFD} = \left| \frac{N \times \sum_{i=1}^{n} N(r_i) r_i - \sum_{i=1}^{n} N(r_i) r_i \sum_{i=1}^{n} r_i}{n \sum_{i=1}^{n} r_i^2 - \left(\sum_{i=1}^{n} r_i\right)^2} \right| \quad (7)$$

After the values of the FFD were obtained in all grid cells, each value was plotted separately at the center of the respective grid to create the contour map and 3D surface map, as shown in Figure 11.

4. METHODOLOGY

4.1. Procedures. The multifactor prediction of the water richness of coal roof aquifers includes four primary steps (Figure 12): (1) the selection of the primary assessment factors, (2) determination of the weights of the assessment factors using the combination weighting method, (3) development of the WRI model using the TOPSIS, and (4) validation of the results and application.

4.2. Building the Hierarchical Structure Model. Based on a previous analysis of the conditioning factors affecting the water richness of the roof aquifers, a hierarchical structure model[22] with a target layer and an indicator layer was developed, as shown in Figure 13. Herein, the target layer of the hierarchy was the water richness of the roof aquifers, and the indicator layer of the hierarchy was formed by seven factors (F_1−F_7): ST, BD, LCI, CR, FSI, FIED, and FFD.

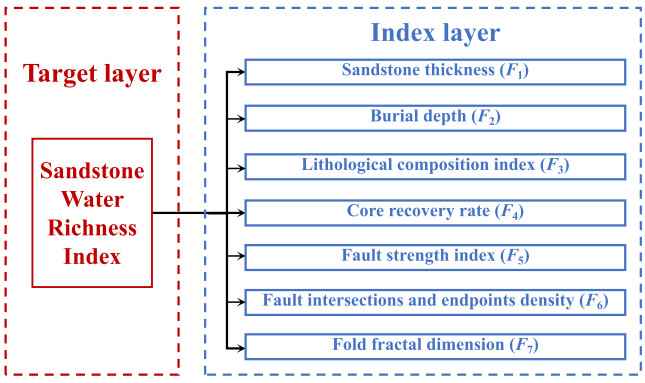

Figure 13. Hierarchical structure model of sandstone water richness.

4.3. Determining Factor Weights. It is crucial to determine the factor weights for developing a water richness prediction model to create a water richness zoning map. Currently, subjective and objective weighting methods are used to determine the factor weights. Both methods have their advantages and disadvantages. The subjective weighting methods are easily influenced by expertise or lack of experience. Although objective weighting methods are based on rigorous mathematical theory and methods to determine the weights, they disregard the subjective orientation and information of the decision maker in the evaluation process. Ideally, the subjective and objective weighting methods should be combined so that the determining factor weights reflect both subjective and objective information. Although a few researchers have conducted studies on comprehensive weight determination, these studies are immature. The existing problems are primarily as follows. The proportion of subjective weight and objective weight in the comprehensive weight is given arbitrarily; the calculation process of the comprehensive weight determination method given is too complicated and the calculation workload is too heavy, which restricts the practical application of the comprehensive weight determination method.

Herein subjective and objective weights were calculated using FDAHP and EWM, respectively, and an optimal combination weight model was developed based on the square sum of deviations to combine the subjective and objective weights.

4.3.1. FDAHP. Many subjective weighting methods, including AHP and FDAHP, were utilized to calculate the factor weights. Herein, FDAHP was used to determine the factor weights. FDAHP integrates fuzzy set theory, AHP, and the Delphi group decision-making method, which is useful for multi-attribution decision-making problems. Compared with AHP, FDAHP in combination with fuzzy set theory can address the fuzziness of human thought and uncertainty in real-world decision-making. FDAHP calculated the factor weights as follows: (1) generating the comparison matrices using the Delphi method; (2) generating the fuzzy pairwise comparison matrix using fuzzy set theory, and (3) determining the factor weights.[23]

Step 1. Generating comparison matrices using the Delphi method.

To determine the factor weights, the relative importance of the seven factors must be determined first using the Delphi method. Based on the hierarchical structure model (Figure 13), the relative importance of each factor was collected from six experts based on the Saaty rating scale, as shown in Table 1.

The pairwise comparison matrices were generated using eq 8:

Table 1. Six Experts' Scores on the Importance of Influencing Factors

	factors						
expert	F_1	F_2	F_3	F_4	F_5	F_6	F_7
1($P1$)	8	6	9	8	7	5	6
2($P2$)	9	8	7	7	8	6	5
3($P3$)	8	7	8	9	6	4	5
4($P4$)	7	9	6	6	8	5	4
5($P5$)	8	5	8	7	9	4	5
6($P6$)	9	7	7	8	8	6	4

https://doi.org/10.1021/acsomega.2c05297
ACS Omega 2022, 7, 44984−45003

$$A = \begin{bmatrix} 1 & a_{12} & a_{13} & a_{14} & a_{15} & a_{16} & a_{17} \\ 1/a_{12} & 1 & a_{23} & a_{24} & a_{25} & a_{26} & a_{27} \\ 1/a_{13} & 1/a_{23} & 1 & a_{34} & a_{35} & a_{36} & a_{37} \\ 1/a_{14} & 1/a_{24} & 1/a_{34} & 1 & a_{45} & a_{46} & a_{47} \\ 1/a_{15} & 1/a_{25} & 1/a_{35} & 1/a_{45} & 1 & a_{56} & a_{57} \\ 1/a_{16} & 1/a_{26} & 1/a_{36} & 1/a_{46} & 1/a_{56} & 1 & a_{67} \\ 1/a_{17} & 1/a_{27} & 1/a_{37} & 1/a_{47} & 1/a_{57} & 1/a_{67} & 1 \end{bmatrix} \quad (8)$$

where $a_{ij} = c_i/c_j$ is the relative importance comparison judgment value for a pair of factors F_i and F_j; $i, j = 1, 2, \ldots, n$, and n is the number of factors. Thus, we got six 7×7 comparison judgment matrices herein as follows:

$$A_{P1} = \begin{bmatrix} 1.00 & 1.33 & 0.89 & 1.00 & 1.14 & 1.60 & 1.33 \\ 0.75 & 1.00 & 0.67 & 0.75 & 0.86 & 1.20 & 1.00 \\ 1.13 & 1.50 & 1.00 & 1.13 & 1.29 & 1.80 & 1.50 \\ 1.00 & 1.33 & 0.89 & 1.00 & 1.14 & 1.60 & 1.33 \\ 0.88 & 1.17 & 0.78 & 0.88 & 1.00 & 1.40 & 1.17 \\ 0.63 & 0.83 & 0.56 & 0.63 & 0.71 & 1.00 & 0.83 \\ 0.75 & 1.00 & 0.67 & 0.75 & 0.86 & 1.20 & 1.00 \end{bmatrix} \quad (9)$$

$$A_{P2} = \begin{bmatrix} 1.00 & 1.13 & 1.29 & 1.29 & 1.13 & 0.50 & 1.80 \\ 0.89 & 1.00 & 1.14 & 1.14 & 1.00 & 1.33 & 1.60 \\ 0.78 & 0.88 & 1.00 & 1.00 & 0.88 & 1.17 & 1.40 \\ 0.78 & 0.88 & 1.00 & 1.00 & 0.88 & 1.17 & 1.40 \\ 0.89 & 1.00 & 1.14 & 1.14 & 1.00 & 1.33 & 1.60 \\ 0.67 & 0.75 & 0.86 & 0.86 & 0.75 & 1.00 & 1.20 \\ 0.56 & 0.63 & 0.71 & 0.71 & 0.63 & 0.83 & 1.00 \end{bmatrix} \quad (10)$$

$$A_{P3} = \begin{bmatrix} 1.00 & 1.14 & 1.00 & 0.89 & 1.33 & 2.00 & 1.60 \\ 0.88 & 1.00 & 0.88 & 0.78 & 1.17 & 1.75 & 1.40 \\ 1.00 & 1.14 & 1.00 & 0.89 & 1.33 & 2.00 & 1.60 \\ 1.13 & 1.29 & 1.13 & 1.00 & 1.50 & 2.25 & 1.80 \\ 0.75 & 0.86 & 0.75 & 0.67 & 1.00 & 1.50 & 1.20 \\ 0.50 & 0.57 & 0.50 & 0.44 & 0.67 & 1.00 & 0.80 \\ 0.63 & 0.71 & 0.63 & 0.56 & 0.83 & 1.25 & 1.00 \end{bmatrix} \quad (11)$$

$$A_{P4} = \begin{bmatrix} 1.00 & 0.78 & 1.17 & 1.17 & 0.88 & 1.40 & 1.75 \\ 1.29 & 1.00 & 1.50 & 1.50 & 1.13 & 1.80 & 2.25 \\ 0.86 & 0.67 & 1.00 & 1.00 & 0.75 & 1.20 & 1.50 \\ 0.86 & 0.67 & 1.00 & 1.00 & 0.75 & 1.20 & 1.50 \\ 1.14 & 0.89 & 1.33 & 1.33 & 1.00 & 1.60 & 2.00 \\ 0.71 & 0.56 & 0.83 & 0.83 & 0.63 & 1.00 & 1.25 \\ 0.57 & 0.44 & 0.67 & 0.67 & 0.50 & 0.80 & 1.00 \end{bmatrix} \quad (12)$$

$$A_{P5} = \begin{bmatrix} 1.00 & 1.60 & 1.00 & 1.14 & 0.89 & 2.00 & 1.60 \\ 0.63 & 1.00 & 0.63 & 0.71 & 0.56 & 1.25 & 1.00 \\ 1.00 & 1.60 & 1.00 & 1.14 & 0.89 & 2.00 & 1.60 \\ 0.88 & 1.40 & 0.88 & 1.00 & 0.78 & 1.75 & 1.40 \\ 1.13 & 1.80 & 1.13 & 1.29 & 1.00 & 2.25 & 1.80 \\ 0.50 & 0.80 & 0.50 & 0.57 & 0.44 & 1.00 & 0.80 \\ 0.63 & 1.00 & 0.63 & 0.71 & 0.56 & 1.25 & 1.00 \end{bmatrix} \quad (13)$$

$$A_{P6} = \begin{bmatrix} 1.00 & 1.29 & 1.29 & 1.13 & 1.13 & 1.50 & 2.25 \\ 0.78 & 1.00 & 1.00 & 0.88 & 0.88 & 1.17 & 1.75 \\ 0.78 & 1.00 & 1.00 & 0.88 & 0.88 & 1.17 & 1.75 \\ 0.89 & 1.14 & 1.14 & 1.00 & 1.00 & 1.33 & 2.00 \\ 0.89 & 1.14 & 1.14 & 1.00 & 1.00 & 1.33 & 2.00 \\ 0.67 & 0.86 & 0.86 & 0.75 & 0.75 & 1.00 & 1.50 \\ 0.44 & 0.57 & 0.57 & 0.50 & 0.50 & 0.67 & 1.00 \end{bmatrix} \quad (14)$$

Step 2. Generating the fuzzy pairwise comparison matrix by fuzzy set theory.

Fuzzy set theory was first introduced by Zadeh[24] and then used for a decision-making problem by Bellman and Zadeh,[25] which can evaluate ambiguity and uncertainty. Fuzzy set theory permits the gradual assessment of the membership of elements in a set, as described by a membership function with a value in the real unit interval $[0, 1]$. TFN[26] is the most prevalent fuzzy set, expressed as $\tilde{M}(s, m, l)$, as shown in Figure 14, where s, m, and l are the minimum and maximum possible values and the most promising value, respectively. The membership function is expressed by eq 15:

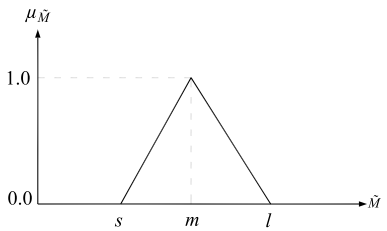

Figure 14. Triangular fuzzy number $\tilde{M}(s, m, l)$.

$$\mu(x|\tilde{M}) = \begin{cases} 0, & x < s, \\ (x - s)/(m - s), & s \le x \le m \\ (l - x)/(l - m), & m \le x \le l \\ 0, & x > l, \end{cases} \quad (15)$$

Herein, the fuzzy pairwise comparison matrix was generated based on six 7×7 comparison matrices using eq 16, as shown in Table 2.

$$\tilde{C} = [\tilde{M}_{ij}] = \begin{bmatrix} (1, 1, 1) & (s_{12}, m_{12}, l_{12}) & \cdots & (s_{1n}, m_{1n}, l_{1n}) \\ (1/s_{12}, 1/m_{12}, 1/l_{12}) & (1, 1, 1) & \cdots & (\alpha_{2n}, \beta_{2n}, \gamma_{2n}) \\ \vdots & \vdots & \ddots & \vdots \\ (1/s_{1n}, 1/m_{1n}, 1/l_{1n}) & (1/s_{2n}, 1/m_{2n}, 1/l_{2n}) & \cdots & (1, 1, 1) \end{bmatrix} \quad (16)$$

https://doi.org/10.1021/acsomega.2c05297
ACS Omega 2022, 7, 44984−45003

Table 2. Fuzzy Pairwise Comparison Matrix

$\tilde{C}$	F_1	F_2	F_3	F_4	F_5	F_6	F_7
F_1	(1.00, 1.00, 1.00)	(0.78, 1.18, 1.60)	(0.89, 1.09, 1.29)	(0.89, 1.09, 1.29)	(0.88, 1.07, 1.33)	(1.40, 1.65, 2.00)	(1.33, 1.70, 2.25)
F_2	(0.63, 0.85, 1.29)	(1.00, 1.00, 1.00)	(0.63, 0.92, 1.50)	(0.71, 0.92, 1.50)	(0.56, 0.90, 1.17)	(1.17, 1.39, 1.80)	(1.00, 1.44, 2.25)
F_3	(0.78, 0.91, 1.13)	(0.67, 1.08, 1.60)	(1.00, 1.00, 1.00)	(0.88, 1.00, 1.14)	(0.75, 0.98, 1.33)	(1.17, 1.51, 2.00)	(1.40, 1.55, 1.75)
F_4	(0.78, 0.91, 1.13)	(0.67, 1.08, 1.40)	(0.88, 1.00, 1.14)	(1.00, 1.00, 1.00)	(0.75, 0.98, 1.50)	(1.17, 1.51, 2.25)	(1.33, 1.55, 2.00)
F_5	(0.75, 0.93, 1.14)	(0.86, 1.11, 1.80)	(0.75, 1.02, 1.33)	(0.67, 1.02, 1.33)	(1.00, 1.00, 1.00)	(1.33, 1.54, 2.25)	(1.17, 1.59, 2.00)
F_6	(0.50, 0.61, 0.71)	(0.56, 0.72, 0.86)	(0.50, 0.66, 0.86)	(0.44, 0.66, 0.86)	(0.44, 0.65, 0.75)	(1.00, 1.00, 1.00)	(0.80, 1.03, 1.50)
F_7	(0.44, 0.59, 0.75)	(0.44, 0.70, 1.00)	(0.57, 0.64, 0.71)	(0.50, 0.64, 0.75)	(0.50, 0.63, 0.86)	(0.67, 0.97, 1.25)	(1.00, 1.00, 1.00)

where s_{ij}, m_{ij}, and l_{ij} indicate the minimum and maximum possible values and the most promising value, respectively; i, j = 1, 2, ..., n, and n is the total number of factors.

Step 3. Determining the factor weights.

First, the fuzzy synthetic extent of the ith factor ($\tilde{S}_i$) was calculated using the following equation:

$$\tilde{S}_i = \tilde{r}_i \otimes (\tilde{r}_1 \oplus \tilde{r}_2 \oplus \cdots \oplus \tilde{r}_n)^{-1} \tag{17}$$

where $\tilde{r}_i = (\tilde{M}_{i1} \otimes \tilde{M}_{i2} \otimes \ldots \otimes \tilde{M}_{in})^{1/n}$; i = 1, 2, ..., n, and n is the total number of factors; and the symbols $\otimes$ and $\oplus$ denote the multiplication and additive operation of fuzzy numbers, respectively.

Consider two TFNs $\tilde{S}_1$ and $\tilde{S}_2$, $\tilde{S}_1 = (s_1, m_1, l_1)$ and $\tilde{S}_2 = (s_2, m_2, l_2)$. The possibility degree of $\tilde{S}_1 \geq \tilde{S}_2$ is defined as follows:

$$P(\tilde{S}_2 \geq \tilde{S}_1) = \sup_{y \geq x}[\min(\mu_{S_1}(x), \mu_{S_2}(y)] = hgt(\tilde{S}_2 \cap \tilde{S}_1) = \mu_{S_2}(d) \tag{18}$$

$$\mu_{S_2}(d) = \begin{cases} 1, \text{ if } m_2 \geq m_1 \\ 0, \text{ if } m_2 < m_1, s_1 \geq l_2 \\ \dfrac{s_1 - l_2}{(m_2 - l_2) - (m_1 - s_1)}, \text{ otherwise} \end{cases} \tag{19}$$

where $P(\tilde{S}_2 \geq \tilde{S}_1)$ denotes the possibility degree of $\tilde{S}_2 \geq \tilde{S}_1$; $\mu_{\tilde{S}_1}$ and $\mu_{\tilde{S}_2}$ are the membership functions of $\tilde{S}_1$ and $\tilde{S}_2$, respectively; and d is the highest ordinate of the crossing point D between $\mu_{\tilde{S}_1}$ and $\mu_{\tilde{S}_2}$,[27] as shown in Figure 15.

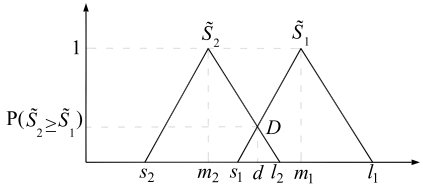

Figure 15. The intersection between $\tilde{S}_1$ and $\tilde{S}_2$.

Subsequently, the possibility degree of a convex fuzzy number $\tilde{S}$ was calculated to be greater than k convex fuzzy number $\tilde{S}_i$ (i = 1, 2, ..., k) using the following equation:

$$\begin{aligned} P(\tilde{S} \geq \tilde{S}_1, \tilde{S}_2, \cdots, \tilde{S}_k) &= P[(\tilde{S} \geq \tilde{S}_1) \text{and} (\tilde{S} \geq \tilde{S}_2) \text{and} \cdots \text{and} (\tilde{S} \geq \tilde{S}_k)] \\ &= \min P(\tilde{S} \geq \tilde{S}_i), \ i = 1, 2, \ldots, k \end{aligned} \tag{20}$$

Additionally, $d(F_j)$ was assumed to be equal to $\min P(\tilde{S}_j \geq \tilde{S}_i)$, where i = 1, 2, ..., n, j = 1, 2, ..., n, and $j \neq i$. Accordingly, the weight vector of factors W' is given by eq 21.[28]

$$W' = (d(F_1), d(F_2), \cdots, d(F_n))^{\mathrm{T}} \tag{21}$$

where F_j is the jth factor; j = 1, 2, ..., n, and n is the total number of factors.

Subsequently, the normalized weight vector was determined via normalization:

$$w = \left(\frac{d(F_1)}{\sum_{i=1}^{n} d(F_i)}, \frac{d(F_2)}{\sum_{i=1}^{n} d(F_i)}, \cdots, \frac{d(F_n)}{\sum_{i=1}^{n} d(F_i)} \right)^{\mathrm{T}} \tag{22}$$

In this step, for the criteria matrix, the values of the fuzzy synthetic extent were obtained according to eq 17:

$$\tilde{S}_1 = (1.001, 1.230, 1.484) \otimes (5.669, 7.135, 9.033)^{-1} = (0.111, 0.172, 0.262)$$

$$\tilde{S}_2 = (0.783, 1.039, 1.453) \otimes (5.669, 7.135, 9.033)^{-1} = (0.087, 0.146, 0.256)$$

$$\tilde{S}_3 = (0.920, 1.124, 1.381) \otimes (5.669, 7.135, 9.033)^{-1} = (0.102, 0.158, 0.244)$$

$$\tilde{S}_4 = (0.913, 1.124, 1.429) \otimes (5.669, 7.135, 9.033)^{-1} = (0.101, 0.158, 0.252)$$

$$\tilde{S}_5 = (0.906, 1.149, 1.492) \otimes (5.669, 7.135, 9.033)^{-1} = (0.100, 0.161, 0.263)$$

$$\tilde{S}_6 = (0.580, 0.745, 0.907) \otimes (5.669, 7.135, 9.033)^{-1} = (0.064, 0.104, 0.252)$$

$$\tilde{S}_7 = (0.567, 0.723, 0.887) \otimes (5.669, 7.135, 9.033)^{-1} = (0.063, 0.101, 0.156)$$

Additionally, the possibility degrees of these fuzzy values were calculated according to eqs 18 and 19:

$$P(\tilde{S}_1 \geq \tilde{S}_2) = 1.000, \ P(\tilde{S}_1 \geq \tilde{S}_3) = 1.000 P(\tilde{S}_1 \geq \tilde{S}_4) = 1.000$$

$$P(\tilde{S}_1 \geq \tilde{S}_5) = 1.000, \ P(\tilde{S}_1 \geq \tilde{S}_6) = 1.000 P(\tilde{S}_1 \geq \tilde{S}_7) = 1.000$$

https://doi.org/10.1021/acsomega.2c05297
ACS Omega 2022, 7, 44984−45003

Table 3. Standardized Matrix

no.	F_1	F_2	F_3	F_4	F_5	F_6	F_7
1	0.204	0.000	0.232	0.789	0.177	0.000	0.000
2	0.200	0.000	0.227	0.854	0.216	0.000	0.000
3	0.215	0.000	0.197	0.893	0.218	0.000	0.000
4	0.362	0.000	0.164	0.112	0.076	0.175	0.000
5	0.326	1.000	0.198	0.121	0.102	1.000	0.000
6	0.243	0.000	0.274	0.206	0.156	0.297	0.000
7	0.200	0.000	0.312	0.478	0.176	0.000	0.000
8	0.245	0.000	0.341	0.779	0.179	0.000	0.922
9	0.159	0.000	0.308	0.845	0.260	0.000	0.000
10	0.172	0.000	0.283	0.856	0.295	0.000	0.000
11	0.198	0.000	0.201	0.894	0.277	0.000	0.000
12	0.237	0.000	0.206	0.890	0.219	0.000	0.000
13	0.457	0.000	0.119	0.211	0.053	0.144	0.000
14	0.445	0.000	0.152	0.365	0.097	0.099	0.864
15	0.366	0.000	0.272	0.496	0.237	0.000	1.000
16	0.242	0.000	0.332	0.576	0.278	0.000	0.000
17	0.212	0.000	0.344	0.663	0.427	0.000	0.000
18	0.142	1.000	0.347	0.718	0.471	0.002	0.000
19	0.065	0.000	0.277	0.758	0.397	0.145	0.000
20	0.117	0.000	0.310	0.791	0.231	0.068	0.000
21	0.636	1.000	0.037	0.443	0.021	0.376	0.000
22	0.352	0.000	0.142	0.543	0.149	0.838	0.000
23	0.091	0.000	0.349	0.400	0.231	0.736	0.000
24	0.238	0.000	0.372	0.456	0.434	0.000	0.000
25	0.178	1.000	0.403	0.544	0.492	0.001	0.000
26	0.087	0.000	0.472	0.499	0.486	0.000	0.000
27	0.041	0.000	0.438	0.537	0.428	0.000	0.000
28	0.092	0.000	0.303	0.572	0.360	0.000	0.000
29	0.313	0.000	0.090	0.739	0.047	0.159	0.922
30	0.200	0.000	0.194	0.764	0.137	0.000	0.864
31	0.172	0.000	0.295	0.707	0.301	0.698	0.730
32	0.250	0.000	0.321	0.670	0.400	0.760	0.000
33	0.271	1.000	0.444	0.593	0.510	0.937	0.000
34	0.106	1.000	0.584	0.461	0.583	0.731	0.000
35	0.166	0.000	0.332	0.496	0.420	0.111	0.000
36	0.307	0.000	0.132	0.676	0.095	0.032	0.000
37	0.285	1.000	0.165	0.752	0.204	0.355	0.000
38	0.109	0.000	0.162	0.745	0.210	0.199	0.730
39	0.198	0.000	0.198	0.814	0.273	0.047	1.000
40	0.375	0.000	0.242	0.773	0.338	0.000	0.922
41	0.327	0.000	0.357	0.647	0.395	0.025	0.609
42	0.299	0.000	0.308	0.556	0.367	0.625	0.000
43	0.281	0.000	0.172	0.542	0.220	0.310	0.000
44	0.397	0.000	0.294	0.593	0.448	0.142	0.000
45	0.139	1.000	0.298	0.736	0.244	0.219	0.000
46	0.092	0.000	0.174	0.729	0.092	0.178	0.000
47	0.302	0.000	0.109	0.753	0.065	0.000	0.000
48	0.449	0.000	0.227	0.748	0.217	0.000	0.000
49	0.350	0.000	0.422	0.612	0.382	0.004	0.000
50	0.426	0.000	0.240	0.555	0.161	0.001	0.000
51	0.131	0.000	0.062	0.409	0.165	0.140	0.000
52	0.089	0.000	0.095	0.495	0.124	0.000	0.000
53	0.197	0.000	0.176	0.512	0.152	0.021	0.000
54	0.564	0.000	0.308	0.486	0.305	0.039	0.000
55	0.262	0.000	0.116	0.443	0.249	0.000	0.000
56	0.233	0.000	0.426	0.373	0.423	0.000	0.000
57	0.416	0.000	0.546	0.363	0.489	0.058	0.000
58	0.381	0.000	0.536	0.371	0.501	0.002	0.000
59	0.064	0.000	0.028	0.267	0.141	0.140	0.000
60	0.000	0.000	0.041	0.300	0.148	0.000	0.000
61	0.149	0.000	0.167	0.313	0.207	0.013	0.000
62	0.310	0.000	0.345	0.289	0.345	0.122	0.000
63	0.465	1.000	0.559	0.253	0.431	0.210	0.000
64	0.238	0.000	0.275	0.093	0.309	0.000	0.000
65	0.434	0.000	0.924	0.124	0.947	0.000	0.000
66	0.458	0.000	1.000	0.205	1.000	0.165	0.000
67	0.331	0.000	0.735	0.250	0.753	0.174	0.000
68	0.037	0.000	0.037	0.217	0.146	0.000	0.000
69	0.023	0.000	0.066	0.162	0.164	0.000	0.000
70	0.104	0.000	0.150	0.201	0.207	0.000	0.000
71	0.241	0.000	0.257	0.184	0.262	0.279	0.000
72	0.342	0.000	0.115	0.110	0.182	0.340	0.000
73	0.278	1.000	0.299	0.000	0.353	0.416	0.000
74	0.325	0.000	0.678	0.013	0.734	0.286	0.000
75	0.367	0.000	0.875	0.095	0.910	0.167	0.000
76	1.000	0.000	0.000	1.000	0.000	0.285	0.000
77	1.000	0.000	0.000	1.000	0.000	0.278	0.000
78	1.000	0.000	0.000	1.000	0.000	0.000	0.000
79	1.000	0.000	0.000	1.000	0.000	0.000	0.000
80	1.000	0.000	0.000	1.000	0.000	0.000	0.000
81	1.000	0.000	0.000	1.000	0.000	0.000	0.000

$P(\tilde{S}_2 \geq \tilde{S}_1) = 0.845$, $P(\tilde{S}_2 \geq \tilde{S}_3) = 0.929 P(\tilde{S}_2 \geq \tilde{S}_4) = 0.929$

$P(\tilde{S}_2 \geq \tilde{S}_5) = 0.910$, $P(\tilde{S}_2 \geq \tilde{S}_6) = 1.000 P(\tilde{S}_2 \geq \tilde{S}_7) = 1.000$

$P(\tilde{S}_3 \geq \tilde{S}_1) = 0.900$, $P(\tilde{S}_3 \geq \tilde{S}_2) = 1.000 P(\tilde{S}_3 \geq \tilde{S}_4) = 1.000$

$P(\tilde{S}_3 \geq \tilde{S}_5) = 0.976$, $P(\tilde{S}_3 \geq \tilde{S}_6) = 1.000 P(\tilde{S}_3 \geq \tilde{S}_7) = 1.000$

$P(\tilde{S}_4 \geq \tilde{S}_1) = 0.905$, $P(\tilde{S}_4 \geq \tilde{S}_2) = 1.000 P(\tilde{S}_4 \geq \tilde{S}_3) = 1.000$

$P(\tilde{S}_4 \geq \tilde{S}_5) = 0.977$, $P(\tilde{S}_4 \geq \tilde{S}_6) = 1.000 P(\tilde{S}_4 \geq \tilde{S}_7) = 1.000$

$P(\tilde{S}_5 \geq \tilde{S}_1) = 0.931$, $P(\tilde{S}_5 \geq \tilde{S}_2) = 1.000 P(\tilde{S}_5 \geq \tilde{S}_3) = 1.000$

$P(\tilde{S}_5 \geq \tilde{S}_4) = 1.000$, $P(\tilde{S}_5 \geq \tilde{S}_6) = 1.000 P(\tilde{S}_5 \geq \tilde{S}_7) = 1.000$

$P(\tilde{S}_6 \geq \tilde{S}_1) = 0.421$, $P(\tilde{S}_6 \geq \tilde{S}_2) = 0.640 P(\tilde{S}_6 \geq \tilde{S}_3) = 0.523$

$P(\tilde{S}_6 \geq \tilde{S}_4) = 0.526$, $P(\tilde{S}_6 \geq \tilde{S}_5) = 0.514 P(\tilde{S}_6 \geq \tilde{S}_7) = 1.000$

https://doi.org/10.1021/acsomega.2c05297
ACS Omega 2022, 7, 44984−45003

Table 4. The Values of Information Entropy and Entropy Weight of each Factor

factors	F_1	F_2	F_3	F_4	F_5	F_6	F_7
information entropy	−0.927	−0.836	−0.931	−0.743	−0.774	−0.524	−0.522
entropy weight	0.157	0.150	0.158	0.142	0.145	0.124	0.124

$$P(\tilde{S}_7 \geq \tilde{S}_1) = 0.391,\ P(\tilde{S}_7 \geq \tilde{S}_2) = 0.611 P(\tilde{S}_7 \geq \tilde{S}_3) = 0.493$$

$$P(\tilde{S}_7 \geq \tilde{S}_4) = 0.496,\ P(\tilde{S}_7 \geq \tilde{S}_5) = 0.484 P(\tilde{S}_7 \geq \tilde{S}_6) = 0.967$$

Consequently, the weight vector of factors was calculated using eqs 20 and 21 as follows:

$$d(F_1) = \min P[(\tilde{S}_1 \geq \tilde{S}_2)\text{and}(\tilde{S}_1 \geq \tilde{S}_3)\text{and}(\tilde{S}_1 \geq \tilde{S}_4)\ \text{and}(\tilde{S}_1 \geq \tilde{S}_5)\text{and}(\tilde{S}_1 \geq \tilde{S}_6)\text{and}(\tilde{S}_1 \geq \tilde{S}_7)] = \min(1.000, 1.000, 1.000, 1.000, 1.000, 1.000) = 1.000$$

$$W' = (1.000, 0.845, 0.900, 0.905, 0.931, 0.421, 0.391)^{\mathrm{T}}$$

Finally, the weight vector was determined after normalization:

$$w = (0.185, 0.157, 0.167, 0.168, 0.173, 0.078, 0.073)^{\mathrm{T}}$$

4.3.2. EWM Approach. Entropy is a measure of the degree of disorder in a system; the lower the degree of disorder, the lower the entropy. EWM is an important application of entropy theory.[29] EWM assigns weights by calculating the amount of information of the factors; the larger the dispersion, the more information it contains, and a higher weight is assigned.[30] Compared with FDAHP, the major advantage of EWM is that it eliminates the interference of subjectivity and ensures the objectivity of weights.[29]

Step 1. Construction of the standardized matrix.

To construct the standardized matrix, the positive correlation factors and negative correlation factors were first normalized using eqs 23 and 24, respectively:

$$r_{ij} = \frac{X_{ij} - X_{\min}}{X_{\max} - X_{\min}} \tag{23}$$

$$r_{ij} = \frac{X_{\max} - X_{ij}}{X_{\max} - X_{\min}} \tag{24}$$

where r_{ij} is the normalized value of the jth factor in the ith assessment sample; $X_{\max}$ and $X_{\min}$ are the maximum and minimum values for the jth factor, respectively; and X_{ij} is the original value of the jth factor in the ith assessment sample. Herein, positive correlation factors include ST, LCI, FSI, FIED, and FFD; negative correlation factors include BD and CR. The greater the value of the positive correlation factor, the stronger the water richness of the roof aquifers, and the greater the value of the negative correlation factor, the weaker the water richness of the roof aquifers.

Subsequently, the standardized matrix $\boldsymbol{R} = \{r_{ij}\}$ was constructed as shown in Table 3.

Step 2. Calculation of the information entropy.

The information entropy of each factor was calculated using the following equation:

$$E_j = -\frac{1}{\ln m} \sum_{i=1}^{m} p_{ij} \ln p_{ij} \tag{25}$$

where $p_{ij} = r_{ij} / \sum_{i=1}^{m} r_{ij}$, E_j is the information entropy of the jth factor, and m is the number of assessment samples.

Step 3. Calculation of the entropy weight.

Based on the calculated entropy of information, the entropy weight of each factor was finally calculated using the following equation:

$$W_j = \frac{1 - E_j}{\sum_{j=1}^{n} (1 - E_j)} \tag{26}$$

where W_j is the entropy weight of the jth factor and n is the number of the factors.

This study comprised 81 assessment samples and seven factors. Thus, an 81 × 7 standardized matrix was constructed using eqs 23 and 24, and the information entropy and entropy weight were obtained as shown in Table 4. Based on the EWM, the weights of ST, BD, LCI, CR, FSI, FIED, and FFD were 0.157, 0.150, 0.158, 0.142, 0.145, 0.124, and 0.124, respectively.

4.3.3. Optimal Combination Weights Model Based on the Square Sum of Deviations. Assuming that there are l methods for assigning weights of n factors and the weight vector given by the kth method is $\boldsymbol{W}_k = [w_{1k}, w_{2k}, ..., w_{nk}]^{\mathrm{T}}$, to synthesize the characteristics of various weighting methods, the following combination weight vector $\boldsymbol{W}_c$ was constructed:

$$\boldsymbol{W}_c = \theta_1 \boldsymbol{W}_1 + \theta_2 \boldsymbol{W}_2 + ... + \theta_l \boldsymbol{W}_l = \boldsymbol{W}\boldsymbol{\Theta} \tag{27}$$

where $\theta_1 \geq 0, \theta_2 \geq 0, ..., \theta_l \geq 0$ are the combination coefficients and $\sum_{k=1}^{l} \theta_k = 1$; $\boldsymbol{W} = [\boldsymbol{W}_1, \boldsymbol{W}_2, ..., \boldsymbol{W}_l]$; $\boldsymbol{\Theta} = [\theta_1, \theta_2, ..., \theta_l]$.

The deviation between the i_1 and i_2 evaluation objects is defined as follows:

$$v_{i_1 i_2}(\boldsymbol{W}_c) = \sum_{j=1}^{n} (y_{i_1 j} - y_{i_2 j}) w_{cj} \tag{28}$$

Additionally, the SSD between the i_1 evaluation objects and the rest is defined as follows:

$$v_i(\boldsymbol{W}_c) = \sum_{i_1=1}^{m} \left[\sum_{j=1}^{n} (y_{ij} - y_{i_1 j}) w_{cj} \right]^2 \tag{29}$$

To maximize the square sum of the total deviations of m evaluation objects, the following objective function was constructed:

https://doi.org/10.1021/acsomega.2c05297
ACS Omega 2022, 7, 44984−45003

$$J(\boldsymbol{W}_c) = \sum_{i=1}^{m} v_i(\boldsymbol{W}_c) = \sum_{i=1}^{m}\sum_{i_1=1}^{m}\left[\sum_{j=1}^{n}(y_{ij} - y_{i_1j})w_{cj}\right]^2$$
$$= \sum_{i=1}^{m}\sum_{i_1=1}^{m}\left[\sum_{j_1=1}^{n}\sum_{j_2=1}^{n}(y_{ij_1} - y_{i_1j_1})w_{cj_1}(y_{ij_2} - y_{i_1j_2})w_{cj_2}\right]$$
$$= \sum_{j_1=1}^{n}\sum_{j_2=1}^{n}\left[\sum_{i=1}^{m}\sum_{i_1=1}^{m}(y_{ij_1} - y_{i_1j_1})(y_{ij_2} - y_{i_1j_2})\right]w_{cj_1}w_{cj_2} \quad (30)$$

Assuming that the matrix $\boldsymbol{Y}_1$ is defined as

$$Y_1 = \begin{bmatrix} \sum_{i=1}^{m}\sum_{i_1=1}^{m}(y_{i1} - y_{i_1 1})(y_{i1} - y_{i_1 1}) & \sum_{i=1}^{m}\sum_{i_1=1}^{m}(y_{i1} - y_{i_1 1})(y_{i2} - y_{i_1 2}) & \cdots & \sum_{i=1}^{m}\sum_{i_1=1}^{m}(y_{i1} - y_{i_1 1})(y_{in} - y_{i_1 n}) \\ \sum_{i=1}^{m}\sum_{i_1=1}^{m}(y_{i2} - y_{i_1 2})(y_{i1} - y_{i_1 1}) & \sum_{i=1}^{m}\sum_{i_1=1}^{m}(y_{i2} - y_{i_1 2})(y_{i2} - y_{i_1 2}) & \cdots & \sum_{i=1}^{m}\sum_{i_1=1}^{m}(y_{i2} - y_{i_1 2})(y_{in} - y_{i_1 n}) \\ \vdots & \vdots & & \vdots \\ \sum_{i=1}^{m}\sum_{i_1=1}^{m}(y_{in} - y_{i_1 n})(y_{i1} - y_{i_1 1}) & \sum_{i=1}^{m}\sum_{i_1=1}^{m}(y_{in} - y_{i_1 n})(y_{i2} - y_{i_1 2}) & \cdots & \sum_{i=1}^{m}\sum_{i_1=1}^{m}(y_{in} - y_{i_1 n})(y_{in} - y_{i_1 n}) \end{bmatrix} \quad (31)$$

Accordingly, the objective function $J(\boldsymbol{W}_c)$ can be expressed as follows:

$$J(\boldsymbol{W}_c) = \boldsymbol{W}_c^{\mathrm{T}}\boldsymbol{Y}_1\boldsymbol{W}_c \quad (32)$$

Thus, the optimal combination weights assignment based on the SSD may be represented as the following optimization problem:

$$\max F(\boldsymbol{\Theta}) = \boldsymbol{\Theta}^{\mathrm{T}}\boldsymbol{W}^{\mathrm{T}}\boldsymbol{Y}_1\boldsymbol{W}\boldsymbol{\Theta} \quad (33)$$

$$\text{s. t.} \begin{cases} \boldsymbol{\Theta}^{\mathrm{T}}\boldsymbol{\Theta} = \boldsymbol{1} \\ \boldsymbol{\Theta} \geq \boldsymbol{0} \end{cases} \quad (34)$$

If $\lambda_{\max}$ is the maximum eigenvalue of the matrix $\boldsymbol{W}^{\mathrm{T}}\boldsymbol{Y}_1\boldsymbol{W}$ and $\boldsymbol{\Theta}^*$ is the unit eigenvector of the maximum eigenvalue, the maximum value of $F(\boldsymbol{\Theta})$ can be denoted as $\lambda_{\max}$, and the optimal solution of the eq 33 can be denoted as $\boldsymbol{\Theta}^*$. When $\boldsymbol{\Theta}^*$ is calculated, the combination weighting $\boldsymbol{W}_c = [w_{cj}]$ can be further calculated using eq 34. Because weight vectors generally meet normalization conditions, the normalized combination weight vector $\boldsymbol{W}_c^*$ can be determined:

$$\boldsymbol{W}_c^* = [w_{cj}^*]^{\mathrm{T}} = \left[w_{cj}/\sum_{j=1}^{n} w_{cj}\right]^{\mathrm{T}} \quad (35)$$

where w_{cj}^* is the normalized combination weight of the j^{th} factor.

Based on the FDAHP and EWM, the subjective weight vector and objective weight vector were $\boldsymbol{W}_1 = [w_{1k}, w_{2k}, \ldots, w_{nk}]^{\mathrm{T}}$, and $\boldsymbol{W}_2 = [w_{1k}, w_{2k}, \ldots, w_{nk}]^{\mathrm{T}}$, respectively. Accordingly, the weight vector $\boldsymbol{W}$ was obtained as follows:

$$\boldsymbol{W} = [\boldsymbol{W}_1, \boldsymbol{W}_2] = \begin{bmatrix} 0.185 & 0.157 & 0.167 & 0.168 & 0.173 & 0.078 & 0.073 \\ 0.157 & 0.150 & 0.158 & 0.142 & 0.145 & 0.124 & 0.124 \end{bmatrix}^{\mathrm{T}}$$

In accordance with the definition of $\boldsymbol{Y}_1$, $\boldsymbol{Y}_1$ was calculated using the MATLAB software as follows:

$$\boldsymbol{Y}_1 = \begin{bmatrix} 56.705 & 18.797 & 53.718 & 5.674 & 5.867 & 9.857 & -16.168 \\ 18.797 & 40.797 & 18.975 & 8.189 & 12.307 & 7.909 & -27.582 \\ 53.718 & 18.975 & 56.864 & 7.269 & 4.265 & 9.439 & -22.824 \\ 5.674 & 8.189 & 7.269 & 16.268 & 0.427 & 1.795 & 5.295 \\ 5.867 & 12.307 & 4.265 & 0.427 & 114.479 & 53.707 & 3.393 \\ 9.857 & 7.909 & 9.439 & 1.795 & 53.707 & 142.000 & -31.248 \\ -16.168 & -27.582 & -22.824 & 5.295 & 3.393 & -31.248 & 473.095 \end{bmatrix}^{\mathrm{T}}$$

Additionally, $\boldsymbol{W}^{\mathrm{T}}\boldsymbol{Y}_1\boldsymbol{W}$ was obtained as follows, based on the vector $\boldsymbol{W}$ and $\boldsymbol{Y}_1$:

$$\boldsymbol{W}^{\mathrm{T}}\boldsymbol{Y}_1\boldsymbol{W} = \begin{bmatrix} 20.171 & 20.423 \\ 20.423 & 22.161 \end{bmatrix}$$

Subsequently, the maximum eigenvalue of the matrix $\boldsymbol{W}^{\mathrm{T}}\boldsymbol{Y}_1\boldsymbol{W}$ was calculated as $\lambda_{\max} = 41.613$, and the unit eigenvector of the maximum eigenvalue is $\boldsymbol{\Theta}^* = [0.690, 0.724]^{\mathrm{T}}$.

Finally, the normalized combination weight vector $\boldsymbol{W}_c^*$ was determined using eq 35:

$$\boldsymbol{W}_{\mathrm{C}} = [0.241 \quad 0.217 \quad 0.230 \quad 0.219 \quad 0.224 \quad 0.144 \quad 0.140]^{\mathrm{T}}$$

$$\boldsymbol{W}_c^* = [0.171 \quad 0.153 \quad 0.162 \quad 0.155 \quad 0.159 \quad 0.101 \quad 0.099]^{\mathrm{T}}$$

4.4. Building the Water Richness Index Model. The TOPSIS method is a multi-attribute decision-making technique applied to a variety of decision-making problems. Herein, the TOPSIS method was used to integrate seven factors to establish WRI using which the water richness of the No. 1 coal seam roof aquifer samples in the study area can be ranked.

https://doi.org/10.1021/acsomega.2c05297
ACS Omega 2022, 7, 44984−45003

Table 5. Water Richness Index of each Assessment Sample

No.	D^-	D^+	WRI	No.	D^-	D^+	WRI
1	0.0299	0.1364	0.1798	42	0.0499	0.1197	0.2941
2	0.0321	0.1358	0.1912	43	0.0303	0.1297	0.1895
3	0.0327	0.1362	0.1934	44	0.0361	0.1277	0.2203
4	0.0173	0.1371	0.1119	45	0.0467	0.1249	0.2723
5	0.0711	0.1220	0.3682	46	0.0278	0.1348	0.1710
6	0.0265	0.1309	0.1684	47	0.0258	0.1402	0.1553
7	0.0251	0.1359	0.1557	48	0.0308	0.1352	0.1857
8	0.0468	0.1122	0.2945	49	0.0370	0.1304	0.2209
9	0.0346	0.1339	0.2053	50	0.0255	0.1364	0.1577
10	0.0349	0.1338	0.2071	51	0.0183	0.1375	0.1174
11	0.0338	0.1353	0.2000	52	0.0178	0.1409	0.1122
12	0.0329	0.1359	0.1946	53	0.0210	0.1379	0.1321
13	0.0170	0.1382	0.1094	54	0.0308	0.1321	0.1891
14	0.0368	0.1166	0.2397	55	0.0209	0.1382	0.1314
15	0.0447	0.1113	0.2867	56	0.0345	0.1312	0.2082
16	0.0300	0.1336	0.1835	57	0.0421	0.1269	0.2493
17	0.0361	0.1314	0.2155	58	0.0418	0.1286	0.2455
18	0.0499	0.1269	0.2823	59	0.0142	0.1396	0.0924
19	0.0361	0.1292	0.2184	60	0.0123	0.1428	0.0796
20	0.0329	0.1327	0.1988	61	0.0176	0.1384	0.1126
21	0.0445	0.1304	0.2546	62	0.0295	0.1302	0.1846
22	0.0562	0.1245	0.3112	63	0.0530	0.1197	0.3070
23	0.0524	0.1214	0.3013	64	0.0228	0.1365	0.1431
24	0.0339	0.1315	0.2052	65	0.0712	0.1249	0.3630
25	0.0496	0.1263	0.2821	66	0.0770	0.1195	0.3918
26	0.0394	0.1299	0.2325	67	0.0580	0.1209	0.3244
27	0.0368	0.1310	0.2193	68	0.0104	0.1432	0.0675
28	0.0308	0.1335	0.1876	69	0.0105	0.1427	0.0685
29	0.1026	0.0946	0.5204	70	0.0151	0.1399	0.0974
30	0.0968	0.0960	0.5023	71	0.0273	0.1300	0.1735
31	0.0950	0.0710	0.5724	72	0.0254	0.1329	0.1603
32	0.0584	0.1175	0.3322	73	0.0482	0.1224	0.2824
33	0.0777	0.1088	0.4167	74	0.0564	0.1204	0.3190
34	0.0722	0.1086	0.3993	75	0.0685	0.1207	0.3619
35	0.0332	0.1293	0.2044	76	0.0431	0.1358	0.2409
36	0.0243	0.1386	0.1491	77	0.0429	0.1359	0.2399
37	0.0480	0.1245	0.2782	78	0.0393	0.1425	0.2163
38	0.0401	0.1140	0.2602	79	0.0393	0.1425	0.2163
39	0.0481	0.1103	0.3039	80	0.0393	0.1425	0.2163
40	0.0476	0.1109	0.3003	81	0.0393	0.1425	0.2163
41	0.0420	0.1147	0.2680				

4.4.1. Constructing the Initial Decision Matrix. Based on the data of the seven factors in all assessment samples, the initial decision matrix was constructed as follows:

$$\boldsymbol{B} = (b_{pj})_{l\times n}\begin{bmatrix} b_{11} & b_{12} & \cdots & b_{1n} \\ b_{21} & b_{22} & & b_{2n} \\ \vdots & \vdots & \ddots & \vdots \\ b_{l1} & b_{l2} & \cdots & b_{ln} \end{bmatrix} \tag{36}$$

where $\boldsymbol{B}$ is the initial decision matrix; l is the number of the assessment samples for water richness assessment of coal roof aquifers; n is the number of the factors, and b_{pj} is the observed value of the j^{th} factor for the p^{th} assessment sample, $j \in [1, n]$ and $p \in [1, l]$.

4.4.2. Constructing the Weighted Standardized Decision Matrix. The decision matrix should be normalized to eliminate the effects of different dimensions and make the data comparable. The standardized decision matrix $\boldsymbol{C}$ was established using eq 37, which can be used for systematic analysis. Subsequently, the weighted standardized decision matrix $\boldsymbol{V}$ was constructed based on the standardized decision matrix $\boldsymbol{C}$ and the normalized combination weight vector $\boldsymbol{W}_c$* as eq 38.

$$\boldsymbol{C} = (c_{pj})_{l\times n} = \left(b_{pj} \Big/ \sqrt{\sum_{p=1}^{j} b_{pj}^2} \right)_{l\times n} \tag{37}$$

where c_{pj} is the j^{th} factor's standardized value of the p^{th} assessment sample.

https://doi.org/10.1021/acsomega.2c05297
ACS Omega 2022, 7, 44984−45003

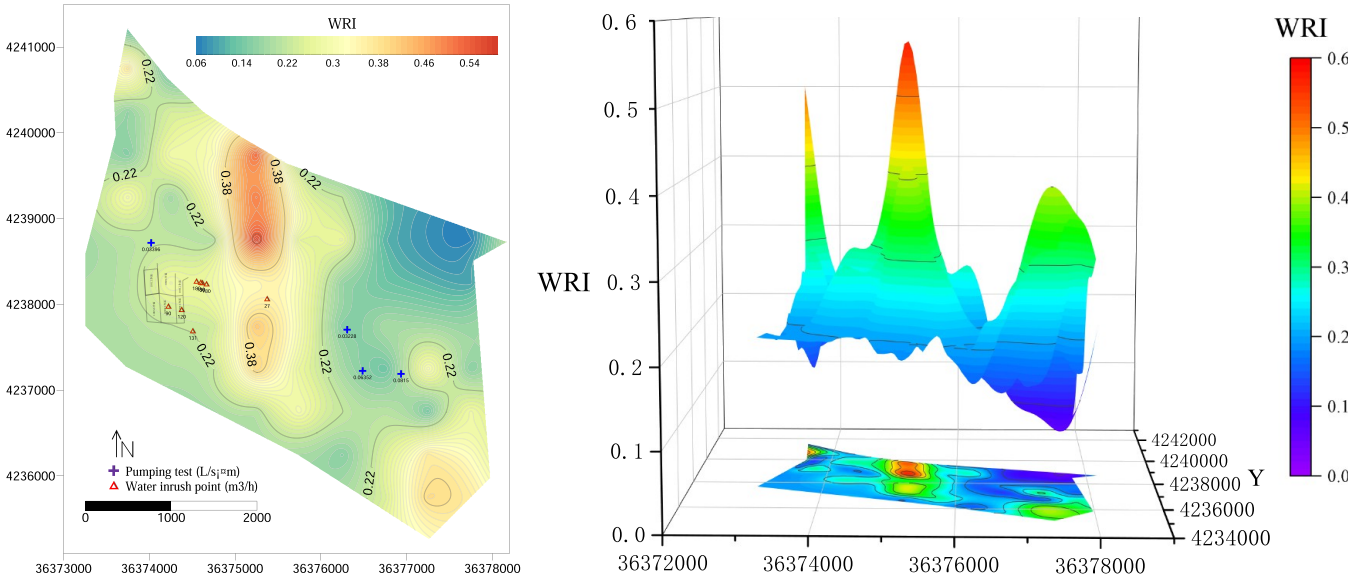

(a) Contour map (b) 3D surface map

Figure 16. Thematic map of sandstone water richness index.

$$\boldsymbol{V} = (v_{pj})_{l\times n} = \begin{bmatrix} w_{c1}^{*}c_{11} & w_{c2}^{*}c_{12} & \cdots & w_{cn}^{*}c_{1n} \\ w_{c1}^{*}c_{21} & w_{c2}^{*}c_{22} & & w_{cn}^{*}c_{2n} \\ \vdots & \vdots & \ddots & \vdots \\ w_{c1}^{*}c_{l1} & w_{c2}^{*}c_{l2} & \cdots & w_{cn}^{*}c_{ln} \end{bmatrix} \tag{38}$$

where $\boldsymbol{V}$ is the weighted normalized decision matrix; v_{pj} is the weighted normalized value of the j^{th} factor of the p^{th} sample; and w_{cj}^{*} is the normalized combination weight of the j^{th} factor.

4.4.3. Determining the Positive Ideal Solution (PIS) and Negative Ideal Solution (NIS). According to the TOPSIS method, the PIS for water richness is an imaginary sample with the strongest water richness of the roof aquifers, and the NIS for water richness is an imaginary sample with the weakest water richness of the roof aquifers. When determining PIS and NIS for the aquifer water richness, the potential positive and negative correlation factors for the water richness must be evaluated independently. The PIS for water richness is a set of the minimum value of the positive factors and the maximum value of the negative factors, while the NIS for water richness is a set of the maximum value of the positive factors and the minimum value of the negative factors, which can be defined as follows:

$$V^{+} = \{(\min_{1\le p\le l} v_{pj} | j \in \boldsymbol{J}_1), (\max_{1\le p\le l} v_{pj} | j \in \boldsymbol{J}_2)\} \tag{39}$$

$$V^{-} = \{(\max_{1\le p\le l} v_{pj} | j \in \boldsymbol{J}_1), (\min_{1\le p\le l} v_{pj} | j \in \boldsymbol{J}_2)\} \tag{40}$$

where V^{+} is the positive ideal solution; V^{-} is the negative ideal solution; v_{pj} is the weighted standardized value of the i^{th} factor of the p^{th} assessment sample; $\boldsymbol{J}_1$ is the set of negative factors; and $\boldsymbol{J}_2$ is the set of positive factors.

4.4.4. Establishing the WRI. The distance of each assessment sample to the PIS and NIS was calculated using eqs 41−42:

$$D_p^{+} = \sqrt{\sum_{j=1}^{n} (v_{pj} - v_j^{+})^2} \tag{41}$$

$$D_p^{-} = \sqrt{\sum_{j=1}^{n} (v_{pj} - v_j^{-})^2} \tag{42}$$

where D_p^{+} is the distance between the p^{th} assessment sample and the PIS; D_p^{-} is the distance between the p^{th} assessment sample and the NIS; v_j^{+} is the value of the j^{th} factor in the set V^{+}; and v_j^{-} is the value of the j^{th} factor in the set V^{-}.

According to the TOPSIS method, the strongest water richness of the roof aquifers would be for the sample that is nearest to the PIS and farthest from the NIS. Therefore, the WRI of the roof aquifers for each assessment sample is defined as follows:

$$\text{WRI}_p = \frac{D_p^{-}}{D_p^{+} + D_p^{-}} \tag{43}$$

where WRI_p is the WRI of the p^{th} assessment sample. The larger the value of WRI, the stronger the water richness of the roof aquifers through which the ranking of water richness of the roof aquifers was determined.

5. RESULTS AND DISCUSSION

5.1. Results. Herein, 81 grid units were created using 500 m × 500 m in each thematic map of the factors, and the data of the seven factors in the 81 grid units were collected to create an 81 × 7 initial decision matrix (Table S1, Supporting Information). The initial decision matrix was standardized using eq 37 and weighted using eq 38 to establish the weighted normalized decision matrix (Table S2, Supporting Information). Herein, BD and CR, being a negative correlation with water richness, belong to set $\boldsymbol{J}_2$; while ST, LCI, FSI, FIED, and FFD being a positive correlation with water richness, belong to set $\boldsymbol{J}_1$. Therefore, based on the weighted normalized decision

https://doi.org/10.1021/acsomega.2c05297
ACS Omega 2022, 7, 44984−45003

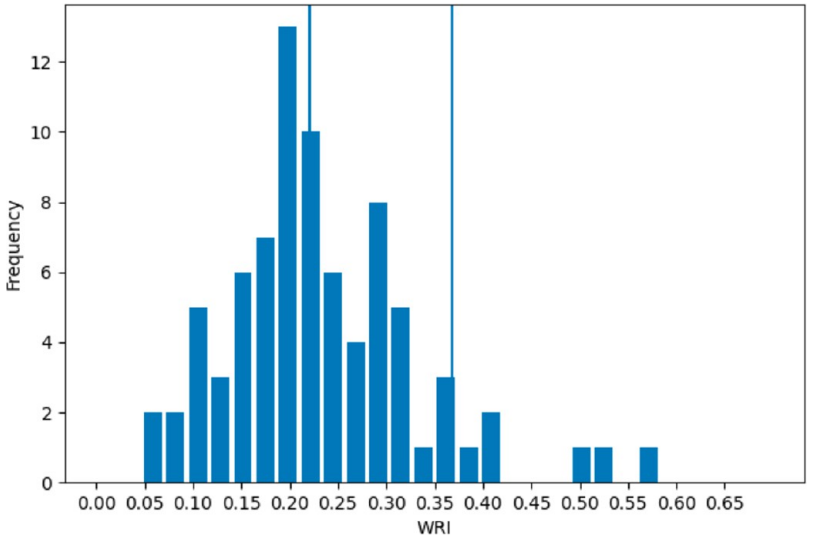

Figure 17. Frequency histogram of the statistical results of WRI values in the study area.

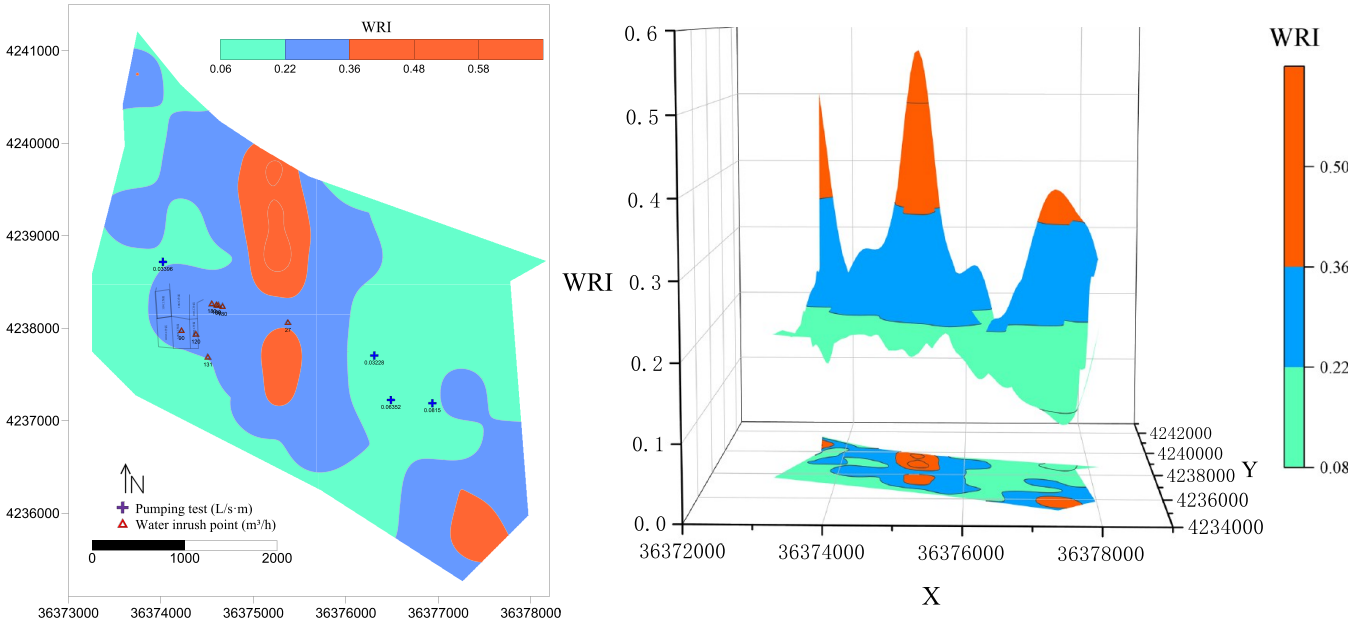

(a) Contour map (b) 3D surface map

Figure 18. Thematic map of sandstone water richness zone.

matrix, the PIS and NIS for the aquifer water richness were calculated using eqs 39−40 as follows:

$$V^{+} = (0.0553, 0.0000, 0.0510, 0.0000, 0.0618, 0.0319, 0.0990)$$

$$V^{-} = (0.0000, 0.0316, 0.0000, 0.0234, 0.0000, 0.0000, 0.0000)$$

The WRI for each assessment sample was finally calculated using eqs 41−43, as shown in Table 5. The data of WRI were processed using Golden Software Surfer 13.0, and a WRI contour map was generated using the kriging function interpolation technique, as shown in Figure 16. In the study area, the WRI value, which indicates the water richness of the No. 1 coal seam roof aquifers, ranged from 0.06 to 0.58.

To partition the water richness of the No. 1 coal seam roof aquifers, the natural breakpoint method (NBM) was used to determine the partition thresholds of the water richness zonation. According to the law of numerical statistical distribution, the NBM is a statistical method of classification that maximizes the difference between classes. There are some natural turning points, characteristic points in any statistical column, by which the study object can be divided into similar groups; so, the breakpoint is a suitable classification threshold.

The frequency histogram of statistical data can assist in determining the natural breakpoint of the data. Figure 17 depicts a frequency histogram of the statistical results of WRI values, and partition thresholds of 0.22 and 0.36 were determined to divide the area into three water richness zones (Figure 18).

https://doi.org/10.1021/acsomega.2c05297
ACS Omega 2022, 7, 44984−45003

Table 6. Validation between Prediction Results by WRI Model and Actual Results

No. of boreholes	q (L/s·m)	Actual results	WRI	WRI prediction results	WRI and actual results comparison
No. S01	0.03396	Weak water richness zone	0.2176	Weak water richness zone	Agree
No. 2803	0.06352	Weak water richness zone	0.1602	Weak water richness zone	Agree
No. 2805	0.08150	Weak water richness zone	0.1897	Weak water richness zone	Agree
No. X3	0.03228	Weak water richness zone	0.1566	Weak water richness zone	Agree

- I: Weak water richness zone: WRI $\leq$ 0.22, mainly located in the northeast and southwest of the study area.
- II: Moderate water richness zone: 0.22 < WRI $\leq$ 0.36, mainly located in the middle, northwest, and southeast of the study area.
- III: Strong water richness zone: WRI > 0.36, mainly located in the north-central part of the study area.

5.2. Validating the Prediction. Validation is essential to verify the predicted results. After obtaining the prediction results, practical engineering data, including pumping tests and water inrushes of the No. 1 coal seam roof aquifers, were processed to validate the results. Herein, validation samples included four pumping tests for the No. 1 coal seam roof aquifers and seven water inrushes at various working faces or roadways, whose locations, names, the data of q obtained via pumping tests, and water inflows of water inrushes are displayed in Figure 18 and Table 6.

As shown in Table 6, based on the data q obtained from pumping tests, the water richness of the four boreholes, Nos. S01, 2803, 2805, and X3, were classified as weak water richness. Similarly, the water richness in the location of the four boreholes, Nos. S01, 2803, 2805, and X3, were predicted as having weak water richness. The results indicate that the prediction results based on the WRI model are consistent with the data from these four pumping tests.

Seven water inrushes occurred in the workfaces of No. 1101S, No. 1102S, No. 1103S, and the +920 tape stone door, with water inflows of 30−180 m^3/h. As shown in Figure 18a, all seven water inrushes fall within the moderate water richness zone based on the WRI model, indicating that the distribution of water inrushes is consistent with the prediction results based on the WRI model.

Therefore, based on the analysis of the pumping tests and the distribution of the water inrushes, the results of the WRI prediction are consistent with practical engineering data, and the WRI prediction is considered accurate and reliable herein.

5.3. Comparison of Predictions by the WRI Model and *q*. According to the Coal Mine Water Control Rules,[16] specific field q derived from pumping test is commonly used to assess the aquifer water richness. As shown in Figure 4, the water richness of the roof aquifers of the No. 1 coal seam in the study area is predicted to be a weak water richness zone based on the data q. However, six medium-sized and one small-sized water inrushes occurred in the weak water richness zone based on the data q. The predictions by q are inconsistent with the characteristics and actual conditions of the water inrush. Based on the distribution of these water inrushes, the prediction accuracy based on q is 0%, whereas the prediction accuracy based on WRI is 100%, indicating that the WRI model performed better than q.

5.4. Discussion. Accurately predicting the water richness zones of roof aquifers is an important and difficult task because of complex geological conditions such as complex lithology distribution, multistage tectonic movement, complex fracture networks, and the anisotropy and heterogeneity of the rock medium. Many factors can affect groundwater storage in sandstone aquifers, and the relationship between these factors and water richness is essential for accurately predicting water richness zones in roof aquifers. Herein, seven factors, including ST, BD, LCI, CR, FSI, FIED and FFD, were used to predict the water richness zones of the No. 1 roof aquifers, and three methods were used to calculate the weights of these factors: FDAHP, EWM, and SSD. The objective weights of these seven factors were calculated using FDAHP, as shown in Figure 19;

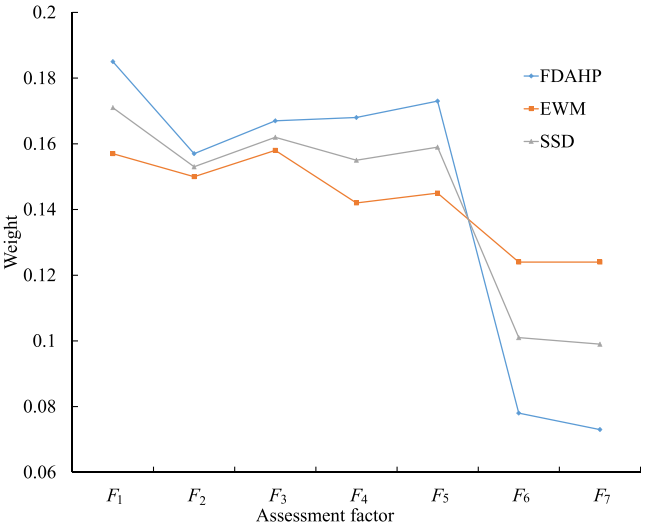

Figure 19. Weighting results by FDAHP, EWM and SSD.

they were 0.185, 0.157, 0.167, 0.168, 0.173, 0.078, and 0.073, respectively. The subjective weights of these seven factors were calculated using EWM, as shown in Figure 19; they were 0.157, 0.150, 0.158, 0.142, 0.145, 0.124, and 0.124, respectively. This indicates that there is a big substantial disparity between the objective and subjective weights of the seven factors. Therefore, the SSD was applied to combine the objective weights and subjective weights, and the optimal combination weights, as shown in Figure 19, were determined to be 0.171, 0.153, 0.162, 0.155, 0.159, 0.101, and 0.099, respectively.

The majority of groundwater storage comprises fissures and fractures developed in the sandstone. The fault and fold factors, including FSI, FIED, and FFD, play a very important role in the distribution of fissures and fractures. The relationship between faults and folds factors and water richness of the No. 1 roof sandstone aquifer was revealed by SSD. With a total weight of 0.359, FSI, FIED, and FFD are considered critical for delineating groundwater richness zones in sandstone aquifers. The more developed the faults and folds, the larger the WRI value and the greater the water richness. As shown in Figures 9, 10, and 11, the distribution of faults and folds is predominantly in a northwest direction, and the distribution directions of moderate and strong water richness zones based on the WRI are also in a northwest direction, as shown in Figure 18, indicating that the distribution of water

https://doi.org/10.1021/acsomega.2c05297
ACS Omega 2022, 7, 44984−45003

richness zones is controlled by the distribution of faults and folds. With a weight of 0.155, the CR factor, which reflects the integrity of a rock mass, plays an important role in the connectivity of groundwater, which is advantageous to the groundwater potential.

With a total weight of 0.514, the development of fissures and fractures and their connectivity are the most important factors affecting groundwater distribution. Additionally, the thickness and lithologies of sandstone are significant because they regulate the total volume of pore and fracture space available for groundwater storage. The LCI indicating the influence of different lithologies on groundwater distribution in sandstone and ST were proposed herein and considered critical when delineating water richness zones in sandstone aquifers, with given weights of 0.162 and 0.171, respectively. With all other factors held constant, as LCI and ST increase, so does the WRI value.

This research accounted for the BD, which influences the water supply, degree of compaction, and secondary porosity. The water supply and available storage spaces for groundwater decrease with increasing depth.[31] The fact that BD weighs 0.153 indicates that it has some effect on water richness.

The water richness of the No. 1 coal roof sandstone aquifers is controlled by seven factors, and a multifactor model of WRI based on the TOPSIS method was established to develop a WRI map. The WRI map shows that groundwater distribution within sandstone aquifers is highly heterogeneous. The practical engineering data including four pumping tests and seven water inrushes were analyzed and successfully validated the WRI model. Compared to the q method, the proposed WRI model, established on the multifactors, performed better in predicting the water richness zones of the No. 1 coal roof sandstone aquifers and can be widely applied to evaluate the water richness of aquifers. The WRI model was established based on the geological and hydrogeological exploration data and several factors related to sandstone water richness. The quality of the WRI model can be improved further with more available data.

6. CONCLUSIONS

Predicting the water richness of coal roof aquifers is essential for the prevention and control of roof water disasters. Meanwhile, accurately predicting water richness zones is a challenging task. The WRI model was proposed and successfully applied to predict the water richness zone of the No. 1 coal roof sandstone aquifers in the Changcheng No. 1 coal mine, China.

The WRI model integrated seven factors, including ST, BD, LCI, CR, FSI, FIED, and FFD. Using FDAHP and EWM , the objective and subjective weights of the seven factors were calculated. The optimal combination weights were determined using the SSD based on objective and subjective weights. ST, BD, LCI, CR, FSI, FIED, and FFD had respective weights of 0.171, 0.153, 0.162, 0.155, 0.159, 0.101, and 0.099. On this basis, the WRI model was developed, and a kriging function interpolation technique was used to create a water richness zone map based on the WRI values. The water richness zones of the No. 1 coal roof sandstone aquifers were classified as weak (WRI $\leq$ 0.22), moderate (0.22 < WRI $\leq$ 0.36), and strong (WRI > 0.36). The prediction zonation obtained using the WRI model was compared to the zonation obtained by the data of q based on the distribution of seven water inrushes, indicating that the WRI model was in good agreement with the field data and performed better at predicting the water richness zones.

ASSOCIATED CONTENT

Supporting Information

The Supporting Information is available free of charge at https://pubs.acs.org/doi/10.1021/acsomega.2c05297.

Initial decision of each assessment sample and Weighted normalized decision of each assessment sample (PDF)

AUTHOR INFORMATION

Corresponding Author

Longqing Shi − *College of Earth Sciences & Engineering, Shandong University of Science and Technology, Qingdao 266590, China;* orcid.org/0000-0002-3845-6973; Email: cattony2002@126.com

Authors

Mei Qiu − *College of Earth Sciences & Engineering, Shandong University of Science and Technology, Qingdao 266590, China*

Xinyu Yin − *College of Earth Sciences & Engineering, Shandong University of Science and Technology, Qingdao 266590, China*

Peihe Zhai − *College of Earth Sciences & Engineering, Shandong University of Science and Technology, Qingdao 266590, China*

Guichao Gai − *College of Earth Sciences & Engineering, Shandong University of Science and Technology, Qingdao 266590, China*

Zhendong Shao − *College of Earth Sciences & Engineering, Shandong University of Science and Technology, Qingdao 266590, China*

Complete contact information is available at: https://pubs.acs.org/10.1021/acsomega.2c05297

Notes

The authors declare no competing financial interest.

ACKNOWLEDGMENTS

We gratefully acknowledge the financial support of the National Natural Science Foundation of China (No. 51804184), the Shandong Province Nature Science Fund (No. ZR2020KE023; and No. ZR2021MD057).

REFERENCES

(1) Jing, G. X., Qin, R. Q.Analysis on the Characteristics of Correlative Factors in Coal Mine Water Disasters from 2011 to 2020. *J. Saf. Environ.* Advance online publication. **2021**, DOI: 10.13637/j.issn.1009-6094.2021.0707.

(2) Li, L. N.; Wei, J. C.; Li, L. Y.; Shi, S. Q.; Yin, H. Y. Water richness prediction model of aquifer based on logging data: an example of Yingpan Trench wellfield in Ordos region. *China Min.* **2019**, *28*, 143−147.

(3) Wu, Q.; Fan, Z. L.; Liu, S. Q.; Zhang, Y. W.; Sun, W. J. Water richness index method based on GIS for information fusion aquifer evaluation. *J. Coal* **2011**, *36*, 1124−1128.

(4) Dai, G. L.; Zhou, Y.; Yang, T.; Liu, M. L.; Gao, Z.; Niu, C. Study on water richness of sandstone of Zhiluo Formation by multi-factor composite analysis. *Coal Sci. Technol.* **2016**, *44*, 186−190.

(5) Li, Z.; Zeng, Y. F.; Liu, S. Q.; Gong, H. J.; Niu, P. K. Application of BP artificial neural network in water richness evaluation. *Coal Eng.* **2018**, *50*, 114−118.

(6) Zhang, H. M.; Wu, J. W.; Zhai, X. R.; Shen, S. H. Fuzzy integrated prediction and evaluation of Water richness of coal-bearing sandstone aquifers–Wolong Lake coal mine seven containment as an example. *Min. Saf. Environ. Prot.* **2018**, *45*, 70−74+79.
(7) Feng, S. S.; Wu, Q. Research on Water richness of aquifers based on the integrated assignment of AHP-variance coefficient method. *Coal En.* **2016**, *48*, 138−140.
(8) Yin, H.; Shi, Y.; Niu, H.; Xie, D.; Wei, J.; Lefticariu, L.; Xu, S. A GIS-based model of potential groundwater yield zonation for a sandstone aquifer in the Juye Coalfield, Shangdong, China. *J. Hydrol.* **2018**, *557*, 434−447.
(9) Zhou, K. Water Richness Zoning and Evaluation of the Coal Seam Roof Aquifer Based on AHP and Multisource Geological Information Fusion. *Geofluids.* **2021**, 1.
(10) Zhang, Y.; Zhang, L.; Li, H.; Chi, B. Evaluation of the Water Yield of Coal Roof Aquifers Based on the FDAHP-Entropy Method: A Case Study in the Donghuantuo Coal Mine, China. *Geofluids.* **2021**, 1.
(11) Huang, S.; Ming, B.; Huang, Q.; Leng, G.; Hou, B. A case study on a combination NDVI forecasting model based on the entropy weight method. *Water Resour. Manage.* **2017**, *31*, 3667−3681.
(12) Sahoo, M. M.; Patra, K. C.; Swain, J. B.; Khatua, K. K. Evaluation of water quality with application of bayes' rule and entropy weight method. *Eur. J. Environ. Civ. Eng.* **2017**, *21*, 730−752.
(13) Dyer, R. F.; Forman, E. H. Group decision support with the analytic hierarchy process. *Decis. Support Syst.* **1992**, *8*, 99−124.
(14) Qin, H.; Luo, D.; Guney, K. New uncertainty measure of rough fuzzy sets and entropy weight method for fuzzy-target decision-making Tables. *J. Appl. Math.* **2014**, *2014*, 487036.
(15) State Bureau of Coal Industry. *Calculation formula for the height of water diversion crack zone for layered mining of thick coal seam. In Regulations for Coal Pillar Retention and Pressed Coal Mining in Buildings, Water Bodies, Railways, and Main Roadways.*; Coal Industry Press. 2017; pp. 56.
(16) State Administration of Coal Mine Safety. *Hydrogeological type of mine. In Coal Mine Water Control Rules.*; Coal Industry Press. 2018; pp. 6.
(17) Zhang, Y. Q.*Forecasting study of water disasters in coal mine under complicated water filling condition--for example the Longgu Coal Mine*; Shandong University of Science and Technology: Qingdao, China. 2008.
(18) Adiat, K. A. N.; Nawawi, M. N. M.; Abdullah, K. Assessing the accuracy of GIS-based elementary multi criteria decision analysis as a spatial prediction tool − A case of predicting potential zones of sustainable groundwater resources. *J. Hydrol.* **2012**, *440-441*, 75−89.
(19) Huang, M.; Yang, B.; Liu, S.; Li, G.; Wu, A. Characteristics of fracture groundwater source and its sublevel drainage system in mines. *Ming R&D.* **2014**, *34*, 59−61+82.
(20) Wang, S. Q.; Wu, C.; Peng, T.; Wu, Z. S.; Liu, K. X. Evaluation of water inrush hazard in roof aquifer of 5-2 coal seam in Qinglongsi coal mine. *J. Xi'an Univ. Sci. Technol.* **2018**, *38*, 959−965.
(21) Shi, L. Q.; Teng, C.; Han, J.; Qiu, M. Evaluation of mine field structure complexity based on analytical hierarchy process and hierarchical cluster analysis. *China Sciencepap.* **2015**, *10*, 2550−2554+2573.
(22) CAI, H.-B. Classification method of deep rock mass based on FDAHP theory. *Hydrogeol. Eng. Geol.* **2012**, *39*, 43−49.
(23) Lima-Junior, F. R.; Osiro, L.; Carpinetti, L. C. R. A comparison between Fuzzy AHP and Fuzzy TOPSIS methods to supplier selection. *Appl. Soft. Comput.* **2014**, *21*, 194−209.
(24) Zadeh, L. A. Fuzzy sets. *Information and Control.* **1965**, *8*, 338−353.
(25) Bellman, R. E.; Zadeh, L. A. Decision-Making in a Fuzzy Environment. *Manage. Sci.* **1970**, *17*, B-141−B-164.
(26) Zhang, S. Y.; Lin, J. Fuzzy decision of hierarchy. *J. Tianjin Univ.* **1989**, *04*, 81−92.
(27) Chang, D. Y. Applications of the extent analysis method on fuzzy AHP. *Eur. J. Oper. Res.* **1996**, *95*, 649−655.
(28) Bangian, A. H.; Ataei, M.; Sayadi, A.; Gholinejad, A. Optimizing post-mining land use for pit area in open-pit mining using fuzzy decision making method. *Int. J. Environ. Sci. Technol.* **2012**, *9*, 613−628.
(29) Yan, F.; Yi, F.; Chen, L. Improved entropy weighting model in water quality evaluation. *Water. Resour. Manag.* **2019**, *33*, 2049−2056.
(30) Zhu, L.; Xing, X.; Yan, F. The Abnormal Phenomena of Entropy Weighting Method in the Dynamic Evaluation of Agricultural Water Conservation. *Math. Probl. Eng.* **2021**, *2021*, 1−5.
(31) Yin, X.; Liu, Q.; Wang, X.; Huang, X. Prediction model of rockburst intensity classification based on combined weighting and attribute interval recognition theory. *J. China Coal Soc.* **2020**, *45*, 3772−3780.

https://doi.org/10.1021/acsomega.2c05297
ACS Omega 2022, 7, 44984−45003